

# NAVAL POSTGRADUATE SCHOOL

## Monterey, California



## THESIS

**DESIGN AND DEVELOPMENT OF THE IMAGE SCANNER  
FOR LINEATE IMAGING NEAR ULTRAVIOLET  
SPECTROMETER (LINUS)**

by

Ricardo C. Kompatzki

December 2000

Thesis Advisor:

D. Scott Davis

Co-Advisor:

Richard C. Olsen

Approved for public release; distribution is unlimited.

<b>REPORT DOCUMENTATION PAGE</b>			Form Approved OMB No. 0704-0188	
Public reporting burden for this collection of information is estimated to average 1 hour per response, including the time for reviewing instruction, searching existing data sources, gathering and maintaining the data needed, and completing and reviewing the collection of information. Send comments regarding this burden estimate or any other aspect of this collection of information, including suggestions for reducing this burden, to Washington headquarters Services, Directorate for Information Operations and Reports, 1215 Jefferson Davis Highway, Suite 1204, Arlington, VA 22202-4302, and to the Office of Management and Budget, Paperwork Reduction Project (0704-0188) Washington DC 20503.				
<b>1. AGENCY USE ONLY (Leave blank)</b>		<b>2. REPORT DATE</b> December 2000	<b>3. REPORT TYPE AND DATES COVERED</b> Master's Thesis	
<b>4. TITLE AND SUBTITLE: DESIGN AND DEVELOPMENT OF THE IMAGE SCANNER FOR LINEATE IMAGING NEAR ULTRAVIOLET SPECTROMETER (LINUS)</b>			<b>5. FUNDING NUMBERS</b>	
<b>6. AUTHOR(S)</b> Kompatzki, Ricardo C.				
<b>7. PERFORMING ORGANIZATION NAME(S) AND ADDRESS(ES)</b> Naval Postgraduate School Monterey, CA 93943-5000			<b>8. PERFORMING ORGANIZATION REPORT NUMBER</b>	
<b>9. SPONSORING / MONITORING AGENCY NAME(S) AND ADDRESS(ES)</b> N/A			<b>10. SPONSORING / MONITORING AGENCY REPORT NUMBER</b>	
<b>11. SUPPLEMENTARY NOTES</b> The views expressed in this thesis are those of the author and do not reflect the official policy or position of the Department of Defense or the U.S. Government.				
<b>12a. DISTRIBUTION / AVAILABILITY STATEMENT</b> Approved for public release; distribution is unlimited.			<b>12b. DISTRIBUTION CODE</b>	
<b>13. ABSTRACT (maximum 200 words)</b>  The Lineate Imaging Near Ultraviolet Spectrometer (LINUS) is a spectral imager that works in the ultraviolet region of the spectrum, and its purpose is to study atmospheric gas plumes. This thesis project is part of an ongoing effort to field-test the first version of LINUS by mid-2001. It concentrates in the development of the ultra-precise servo system that controls the pointing/scanning system of the instrument. The closed-loop angular-position servo is controlled by a dedicated motion controller board that is installed in the host computer. Control of the servo is achieved through proportional-integral-derivative (PID) algorithms built into the hardware and firmware of the motion controller board. The servo has been designed to an angular resolution of 9 seconds of arc, and was tuned for a step of 1000 counts. Static and dynamic tests were conducted and showed that the servo is stable and accurate. The tested accuracy of the servo is well within the design goal of one half encoder count.				
<b>14. SUBJECT TERMS</b> Sensors, Spectral Imaging, Spectrometer, Remote Sensing			<b>15. NUMBER OF PAGES</b>	
			<b>16. PRICE CODE</b>	
<b>17. SECURITY CLASSIFICATION OF REPORT</b> Unclassified	<b>18. SECURITY CLASSIFICATION OF THIS PAGE</b> Unclassified	<b>19. SECURITY CLASSIFICATION OF ABSTRACT</b> Unclassified	<b>20. LIMITATION OF ABSTRACT</b> UL	

THIS PAGE INTENTIONALLY LEFT BLANK

Approved for public release; distribution is unlimited.

**DESIGN AND DEVELOPMENT OF THE IMAGE SCANNER FOR LINEATE  
IMAGING NEAR ULTRAVIOLET SPECTROMETER (LINUS)**

Ricardo C. Kompatzki  
Lieutenant, Navy of Chile  
B.S., Navy of Chile Polytechnic Academy, 1994

Submitted in partial fulfillment of the  
requirements for the degree of

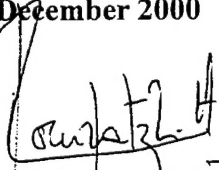
**MASTER OF SCIENCE IN APPLIED PHYSICS**

from the


**NAVAL POSTGRADUATE SCHOOL**

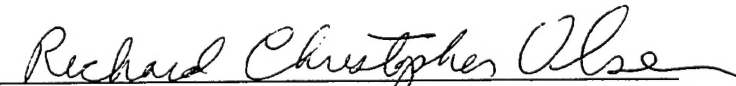
**December 2000**

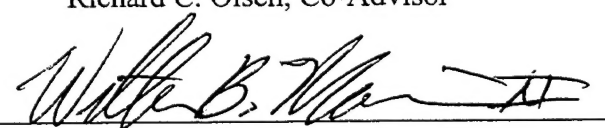
Author:

  
Ricardo C. Kompatzki

Approved by:

  
D. Scott Davis, Thesis Advisor

  
Richard C. Olsen, Co-Advisor

  
William B. Maier II, Chairman  
Department of Physics

THIS PAGE INTENTIONALLY LEFT BLANK

## **ABSTRACT**

The Lineate Imaging Near Ultraviolet Spectrometer (LINUS) is a spectral imager that works in the ultraviolet region of the spectrum, and its purpose is to study atmospheric gas plumes. This thesis project is part of an ongoing effort to field-test the first version of LINUS by mid-2001. It concentrates in the development of the ultra-precise servo system that controls the pointing/scanning system of the instrument. The closed-loop angular-position servo is controlled by a dedicated motion controller board that is installed in the host computer. Control of the servo is achieved through proportional-integral-derivative (PID) algorithms built into the hardware and firmware of the motion controller board. The servo has been designed to an angular resolution of 9 seconds of arc, and was tuned for a step of 1000 counts. Static and dynamic tests were conducted and showed that the servo is stable and accurate. The tested accuracy of the servo is well within the design goal of one half encoder count.

THIS PAGE INTENTIONALLY LEFT BLANK

## TABLE OF CONTENTS

<b>I.</b>	<b>INTRODUCTION.....</b>	<b>1</b>
A.	<b>OBJECTIVE .....</b>	<b>2</b>
B.	<b>OUTLINE .....</b>	<b>3</b>
<b>II.</b>	<b>BACKGROUND .....</b>	<b>5</b>
A.	<b>OVERVIEW .....</b>	<b>5</b>
B.	<b>THE BASIC PHYSICS OF LINUS'S SPECTROSCOPIC DESIGN...</b>	<b>6</b>
C.	<b>THE IMAGING CONCEPT.....</b>	<b>12</b>
D.	<b>THE LINUS SCANNING OPTICS.....</b>	<b>13</b>
<b>III.</b>	<b>HARDWARE AND SOFTWARE OVERVIEW .....</b>	<b>17</b>
A.	<b>HOST COMPUTER.....</b>	<b>19</b>
B.	<b>CAMERA.....</b>	<b>20</b>
C.	<b>SERVO SYSTEM .....</b>	<b>25</b>
D.	<b>OPTICS.....</b>	<b>27</b>
E.	<b>SOFTWARE.....</b>	<b>28</b>
<b>IV.</b>	<b>THE SERVO-SYSTEM .....</b>	<b>31</b>
A.	<b>SERVO SYSTEM BASICS.....</b>	<b>31</b>
B.	<b>INTERFACING THE COMPONENTS.....</b>	<b>33</b>
C.	<b>DRIVING THE LOAD.....</b>	<b>36</b>
D.	<b>TUNING THE SERVO .....</b>	<b>39</b>
<b>V.</b>	<b>TEST RESULTS .....</b>	<b>43</b>
A.	<b>DYNAMIC STEPPING TESTS .....</b>	<b>43</b>
B.	<b>STATIC STABILITY TEST.....</b>	<b>46</b>
C.	<b>POINTING ACCURACY TEST .....</b>	<b>48</b>
D.	<b>IMAGING TEST ATTEMPTS .....</b>	<b>50</b>
<b>VI.</b>	<b>CONCLUSIONS .....</b>	<b>53</b>
	<b>APPENDIX A. HARDWARE DATA .....</b>	<b>55</b>
	<b>APPENDIX B. LABVIEW PROGRAMS.....</b>	<b>75</b>
	1. <b>LINUS INITIALIZATION.VI.....</b>	<b>75</b>
	2. <b>LINUS STEPPING PROGRAM.VI.....</b>	<b>80</b>
	<b>APPENDIX C. SERVO TUNING PROCEDURE.....</b>	<b>83</b>
	<b>LIST OF REFERENCES .....</b>	<b>85</b>
	<b>INITIAL DISTRIBUTION LIST .....</b>	<b>87</b>



THIS PAGE INTENTIONALLY LEFT BLANK

## **ACKNOWLEDGMENTS**

The author would like to thank Dr. Scott Davis for his permanent guidance, support and trust during this thesis project. The author would also like to thank his wife Pamela and his son Ricardo for their love and patience.

THIS PAGE INTENTIONALLY LEFT BLANK

## I. INTRODUCTION

The research project described in this thesis has dealt with the initial design and development of LINUS (Lineate Imaging Near Ultraviolet Spectrometer), an ultraviolet imaging spectrometer dedicated to studying atmospheric gas plumes. It is a continuation of several years of research and engineering at the Naval Postgraduate School's Department of Physics.

LINUS can trace its origins back to 1990, when another instrument, MUSTANG (Middle Ultraviolet SpecTrograph for Analysis of Nitrogen Gases), was designed to analyze the earth's ionosphere. MUSTANG was a conventional spectrometer, incapable of spectroscopic imaging. In 1996 an attempt to convert MUSTANG from a spectrograph to an imaging spectrometer was conducted. The result of this effort was DUUVIS (Dual Use UltraViolet Imaging Spectrometer), a hybrid design which appended the MUSTANG optics to a scanning imaging system. During early 1997 DUUVIS was tested, but it did not generate acceptable quality images. As a result, design and development of an entirely new instrument, NUVIS (Naval Postgraduate School UltraViolet Imaging Spectrometer) was undertaken. This was not a hybrid or add-on instrument. It was conceived as a stand-alone ultraviolet imaging spectrometer from the outset. In the interest of cost-control, however, it did incorporate some of the optical components from MUSTANG. The design and fabrication of this new instrument was completed in the fall of 1997. To test it, the designers decided that they would measure the ability of the instrument to analyze and characterize a chemical effluent plume in the field. This effort was conducted in two parts, first by Dr. David Cleary and then by Dr.

Scott Davis during 1998 and 1999. The initial field trials involved observations of volcanic plumes in Hawaii and combustion plumes from industrial smokestacks. This earlier effort was plagued by poor weather and logistical problems, and has remained largely unanalyzed and inconclusive. The follow-on work by Marino [1] was more definitive. The results of his work conclusively demonstrated the ability of NUVIS to detect and quantify SO<sub>2</sub> emissions flowing out of a smokestack, produced by the industrial burning of coal. NUVIS detected the SO<sub>2</sub> by means of the molecule's spectral absorption against scattered ultraviolet sunlight.

The field and laboratory measurements made during Marino's research revealed several limitations with NUVIS's optical design, detection system and control hardware/software. Rather than modifying or improving NUVIS, it was decided to develop a third-generation instrument. This decision was reached because the NUVIS design will always be rigidly constrained to marginal measurements of SO<sub>2</sub> only; it cannot be adapted to more varied, and potentially more productive, applications. Hence, the LINUS project was conceived in late 1999-early 2000 as an instrument to overcome NUVIS's shortfalls.

#### **A. OBJECTIVE**

This thesis project has been part of an ongoing effort to field-test the first version of LINUS by mid-2001. The motivation to work in the development of this project comes from the author's personal interest in electro-optical systems and a fascination with the detailed engineering of such systems. At the time that this thesis project was begun, LINUS existed only as a proposed project, with few design details and no actual

hardware or software in place. Thus, the thesis work has constantly evolved and adapted as the initial design phases of the project have taken place.

It was recognized at the outset that LINUS's most radical design departures from its predecessors would be in two areas: its optomechanical image scanning system and the field-deployable computer hardware and software that will actively control the instrument. Therefore, the development of the two subsystems were chosen as the topics for this thesis project.

## **B. OUTLINE**

This thesis is composed of six chapters and three appendices. Chapter II gives a brief overview of the optical physics and mechanics involved in an imaging spectrometer, and the characteristics of the output data. Chapter III describes the architecture of the computer system that has been assembled and details of the actual hardware and software components. Chapter IV describes the development of the optomechanical image scanning servo system, and the process of integrating the servo system with the host computer. Chapter V shows the results of various tests and figure-of-merit measurements of the servo subsystem. Conclusions and recommendations for follow-on work are contained in Chapter VI. The appendices contain various supporting documentation giving specific design details and performance information for the project.

THIS PAGE INTENTIONALLY LEFT BLANK

## II. BACKGROUND

### A. OVERVIEW

Spectral imaging is a remote sensing technique that has both civilian and military applications. Historically, there was a distinction between purely spectroscopic and purely imaging techniques. Spectroscopy concerns itself with the analysis of the wavelength (or, equivalently frequency) dependence of the intensity distribution of an electromagnetic radiation field, with little or no concern for the directional or spatial dependence of the field. Under favorable circumstances, spectra can reveal a great deal of information about chemical composition, temperature and surface properties of a radiation source, as well as the intervening source-to-sensor medium. Pure imaging, on the other hand, deals only with the amount of radiation coming from different portions of a scene (also called picture elements, or pixels) with minimal attention paid to spectral information.

Spectral imaging is a fairly recent technique which strives to combine the two methods, recording the image scene as a set of spectra on a pixel-by-pixel basis. This means that a spectral image is inherently a more complicated entity than a spectrum or an image alone. The resulting data set is generally expressed as measured irradiance as a function of three independent variables: 2 spatial coordinates expressing each pixel's position in the image field, plus 1 spectral coordinate, such as wavelength, frequency or wavenumber. Because optical detectors are necessarily planar devices, capable of measuring only a single pixel (a so-called discrete detector), a linear strip of pixels (called linear array detectors) or a mosaic of pixels in two dimensions (colloquially



known as focal plane array), spectral imagers must resort to extraordinary means to measure the three dimensional character of their data.

The basic optical and optoelectronic operations of pure spectroscopy and pure imaging are summarized in the following sections. Then a discussion of how they are combined into the LINUS design is presented.

## **B. THE BASIC PHYSICS OF LINUS'S SPECTROSCOPIC DESIGN**

The purpose of any modern purely spectroscopic instrument is to measure the radiant power from a source as a function of wavelength or frequency, and to convert that optical measurement first into electronic and ultimately into digital form for processing and display via computer. A huge variety of different instruments exists, but in the end, almost all of them rely on one or more of five basic means of decomposing an optical radiation field into its spectral components. Three of the five are direct descendents of the pre-electronic age and were perfected in the days when the dominant photo detection technology was photochemical (i.e. photography) instead of optoelectronic. They are, in historical order: (1) photodispersive devices (i.e. prism-based spectrometers), (2) wavefront division multiple-beam interferometers (i.e. diffraction gratings), and (3) amplitude-division multiple-beam interferometers (i.e. Fabry-Perot interferometers). The other two spectroscopic methods are more modern, and include ultra-high resolving power two-beam interferometers (i.e. Fourier transform spectroscopy) and nonlinear optical heterodyning devices. Detailed descriptions of the basic physics of these techniques may be found in a variety of references [2; 3; 4; 5; 6]. Each method has its technical strengths and weaknesses, and, by means of careful design, can be adapted to an

imaging system to produce a spectral imager. For reasons of simplicity, speed of development and economics, it was decided that the spectroscopic subsystem of LINUS would be based upon a conventional plane diffraction grating. What follows is an outline of how such device works.

LINUS uses the physical process known as far-field or Fraunhofer diffraction. Even though LINUS uses a reflective diffraction grating, a transmission grating will be used to illustrate the fundamental principle involved.

Figure 2.1 shows the setup. From left to right, collimated light of wavelength  $\lambda$  coming from a scene of interest, is transmitted through the diffraction grating. The grating is simply an array of equally-spaced apertures. The optical properties of the output beam are the simplest when the output plane is located at distance  $R$  from the center of the grating.  $R$  satisfies the condition [2]

$$R > \frac{a^2}{\lambda}, \quad (2.1)$$

so that the diffracted beam is in the far-field regime when it reaches the output plane.

Let us suppose that the grating is composed of  $N$  identical slits of width  $b$ . Furthermore, let the distance between centers of adjacent slits be  $a$ .

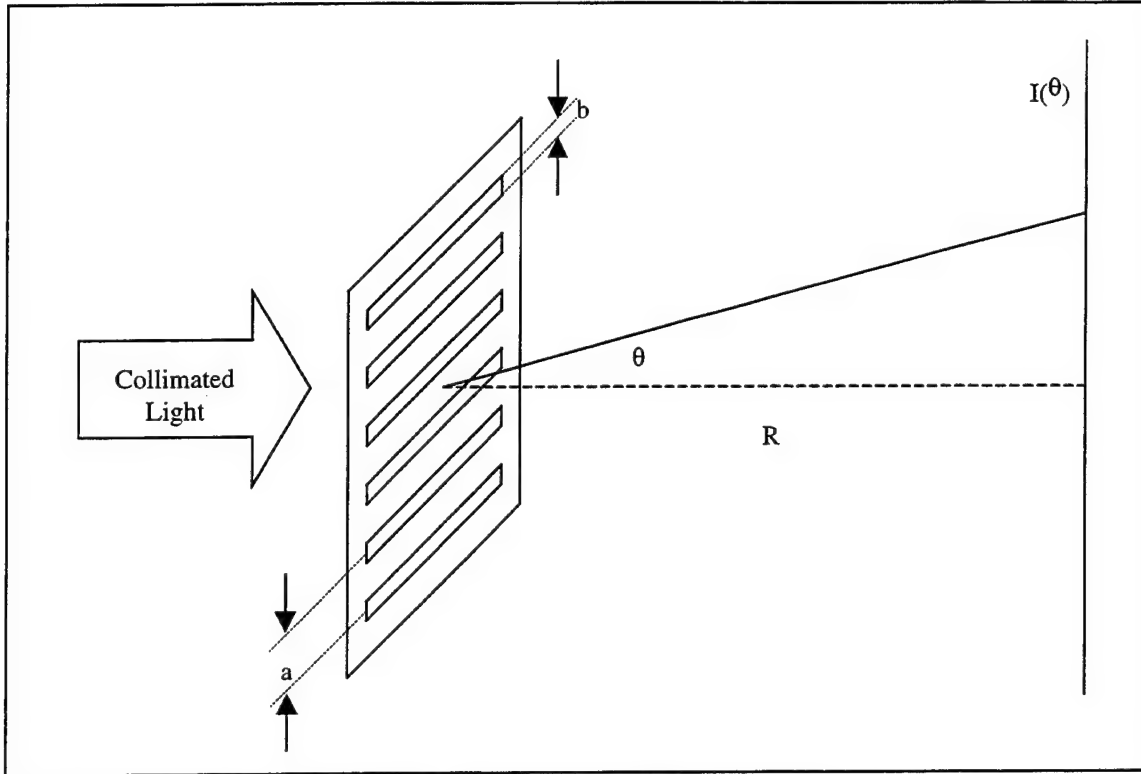


Figure 2.1. The far-field diffraction setup.

Analysis of the resulting interference (diffraction) pattern then shows that the flux-density distribution function at the output plane is given by [2]

$$I(\theta) = I_0 \left( \frac{\sin \beta}{\beta} \right)^2 \left( \frac{\sin N\alpha}{\sin \alpha} \right)^2, \quad (2.2)$$

where  $I_0$  is the incident flux density of the electromagnetic radiation in the  $\theta = 0$  direction and

$$\beta = \frac{\pi b}{\lambda} \sin \theta \quad (2.3)$$

and

$$\alpha = \frac{\pi a}{\lambda} \sin \theta \quad (2.4)$$

The symbol  $\lambda$  denotes the wavelength of the radiation in the medium between the grating and the output plane. Since LINUS will operate in ambient air, this is simply the radiation's vacuum wavelength divided by the (wavelength-dependant) refractive index of air. From Equation 2.4 it can be easily shown that the flux density maxima occur at specific angles satisfying

$$\theta_m = \arcsin\left(\frac{m\lambda}{a}\right), \quad (2.5)$$

where  $m$  is any integer, positive, negative, or 0, that yields a real angle.  $m$  is called the order number of the diffraction pattern. From this result it can be seen that the zeroth-order maximum ( $m = 0$ ) will be at  $\theta = 0$  independent of the wavelength of the incoming light. Hence, all incident wavelengths will appear in the zeroth-order diffraction pattern. On the other hand, for higher-order maxima ( $|m| > 0$ )  $\theta_m$  will vary with wavelength, being larger for longer wavelengths. That is, different wavelength components of the radiation field will then propagate at different angles. They are said to be angularly dispersed.

Equation 2.2 is plotted in Figure 2.2 to illustrate its general shape. The maxima for  $m=0, 1$ , and  $2$  are shown. It is evident that if the flux density at the output plane can be measured as a function of  $\theta$ , then a measure of the spectrum of the light diffracted by the grating will be obtained.

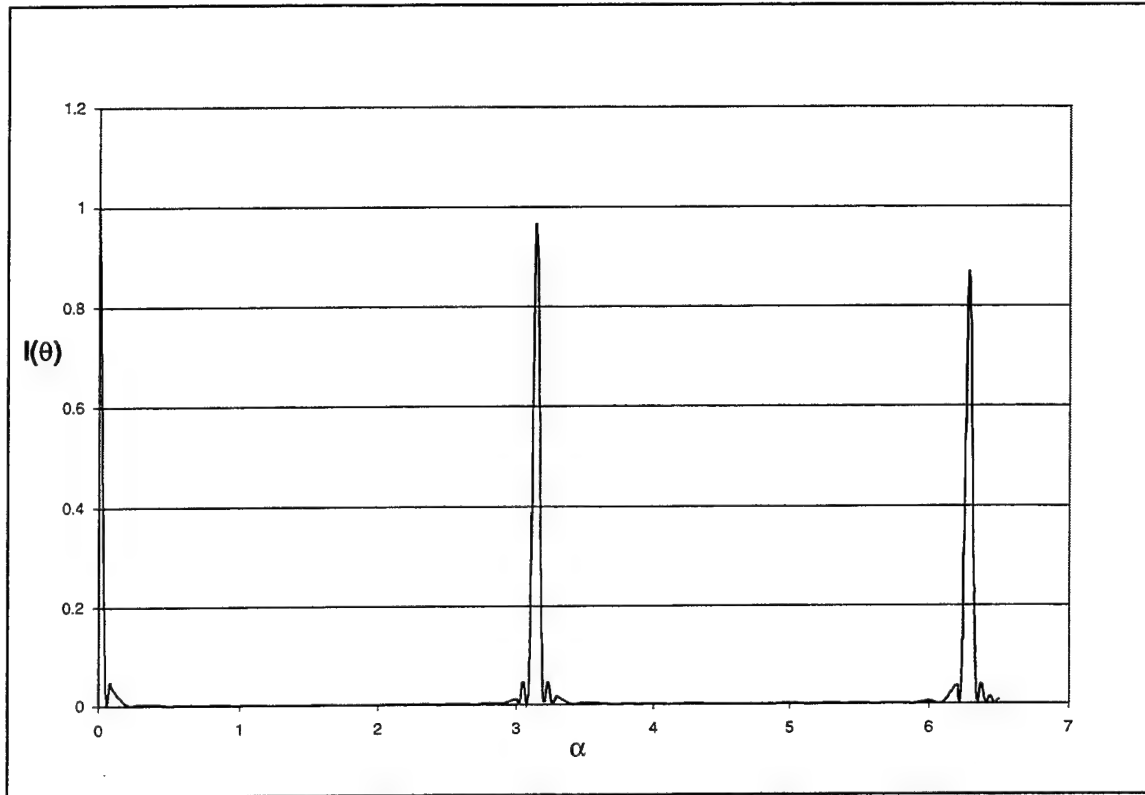


Figure 2.2. Diffraction pattern showing the first 3 maxima.

It can also be shown that the limit of resolution for this system, using Rayleigh's criterion [2], is given by

$$\Delta\lambda_{\min} = \frac{\lambda}{mN}, \quad (2.6)$$

where  $\Delta\lambda_{\min}$  is the least resolvable wavelength difference at mean wavelength  $\lambda$ , and  $N$  is the number of slits defined earlier. This result shows that the higher the order of diffraction used and the more slits illuminated, the finer will be the resolution. But, for unambiguous spectroscopic measurements, the order cannot be chosen arbitrarily high, because of a phenomenon called order overlapping. Referring back to Equation 2.5, one can readily see that it is possible for spectral features of different wavelengths to coincide

in diffracted angle, provided they both satisfy Equation 2.5, and therefore have different orders. For example, a first order 600 nm line will be diffracted at the same angle as a second order 300 nm line. This will result in a complete superposition, or blending, of the two spectral features. The larger the measurable bandwidth required, the lower the order that must be used. Because of this tradeoff, a low order maximum is usually chosen to obtain larger bandwidth. The implication for resolution, is that  $N$  must be increased to obtain the desired value. In the end, the resolution is limited by the finite number of slits, or rulings, on the grating.

Once the radiation field of interest has been diffracted by a grating, it is a straightforward procedure to measure the spectrum. A focusing apparatus (effectively a telescope objective lens or mirror) is illuminated by the diffraction pattern, as shown in Figure 2.3.

Collimated radiation entering the objective at an angle  $\theta$  relative to the optical axis will be brought to a focus on the focal plane, at a distance

$$x = f \cdot \tan \theta \approx f \cdot \sin \theta \approx f \cdot \theta \quad (2.7)$$

from the optical axis. Here,  $f$  is the effective focal length of the objective and the paraxial, small angle approximation  $\tan \theta \approx \sin \theta \approx \theta$  may be used as appropriate. Of course, optical aberrations [2] will always be present, and care must be taken in designing the optics if they are to be reduced to a tolerable level.

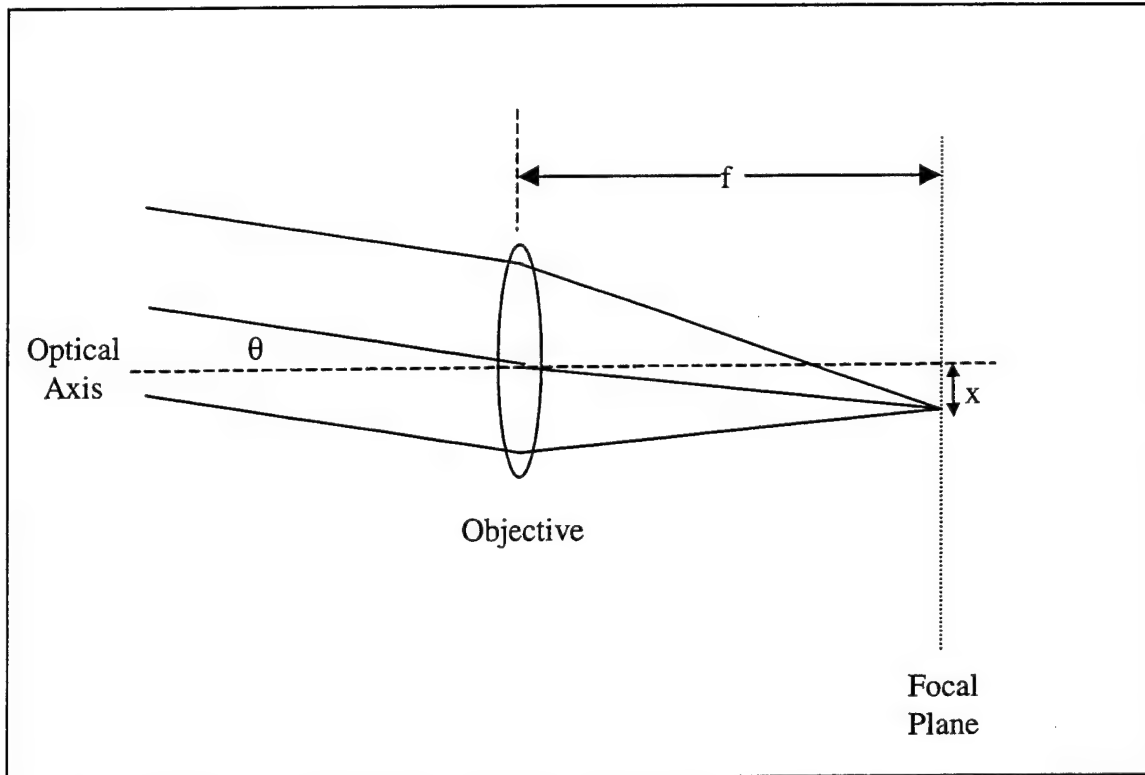


Figure 2.3. Collimated radiation entering the objective at an angle  $\theta$ .

Finally, an optoelectronic detector is placed in the focal plane. A simple discrete detector will not do in this instance. Because the spectrum is dispersed in the  $x$ -direction, either a linear array or focal plane array of extended size is required.

### C. THE IMAGING CONCEPT

In remote sensing applications, radiation sources are, by definition, located far from the sensing apparatus or instrument. Therefore, the optical configuration for an imager is essentially the same one as shown in Figure 2.3, above. Because the optical waves arriving from a distant source are essentially collimated and planar, a telescope objective lens or mirror will focus the radiation originating from different points on the source onto distinct points on the focal plane (again, ignoring aberrations and objective

aperture diffraction effects). A two-dimensional detector array placed at the objective's focal plane will then record an image.

Recall, however that a spectral imager records data dependant upon three variables: the two spatial coordinates of image pixel points and one spectral coordinate, usually wavelength. The resulting data set is usually displayed arrayed in a three-dimensional Cartesian coordinate system, shown in Figure 2.4. The best that an inherently 2-D array detector can do is to record one layer of this cube at a time. Hence, at least one of the spectral data cube's coordinate axes must be successively scanned in order to produce a spectral image. In LINUS, one of the detector's spatial axes is allocated to detecting the angularly dispersed spectral information, while its orthogonal axis is assigned to one of the image's spatial directions. The other image dimension is then sequentially scanned via an optomechanical scanning system.

#### **D. THE LINUS SCANNING OPTICS**

The mechanism to build the spectral cube chosen for LINUS is schematically shown in Figure 2.5. The optics of the instrument are designed to focus one vertical strip of the scene onto the spectrometer's entrance slit at a time. Light from this vertical strip is captured by the optics and collimated so that radiation from each vertically spaced pixel reaches the diffraction grating in the plane wave regime, but is fanned out vertically. The grating's rulings are oriented vertically also, causing angular dispersion in the horizontal plane as described in section B. A second objective optical system then focuses the radiation onto a 2-D detector array in the output plane. The resulting image is



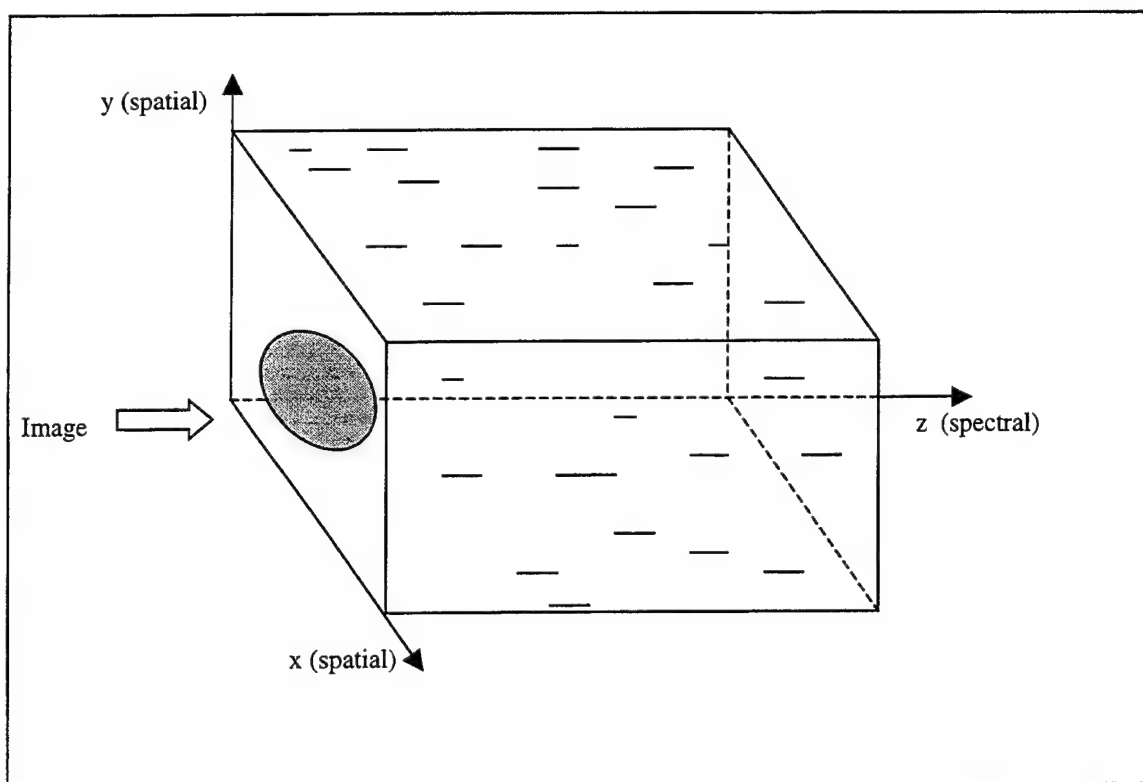


Figure 2.4. The spectral cube.

comprised of a stacked set of spectra, dispersed horizontally, one for each vertically positioned pixel along the entrance slit. In other words, the optics are stigmatic (shape-preserving), so that the image appears as a horizontally dispersed set of vertical slit images, one for each wavelength. After being captured, the frame of data is read out from the detector for processing.

In order to acquire complete 3-D image scene data, the telescope must be pointed sequentially at neighboring vertical strips of the target field. This technique is known as a “pushbroom” imager [7]. Building the spectral cube can be visualized as the stacking of frames shown in Figure 2.6. In the LINUS instrument, the successive pointing of the telescope optics towards neighboring strips of the image is accomplished by a plane

steering mirror, positioned in front of the telescope. Development of the ultra-precise servo system to control this pointing/scanning system has constituted the bulk of this thesis project.

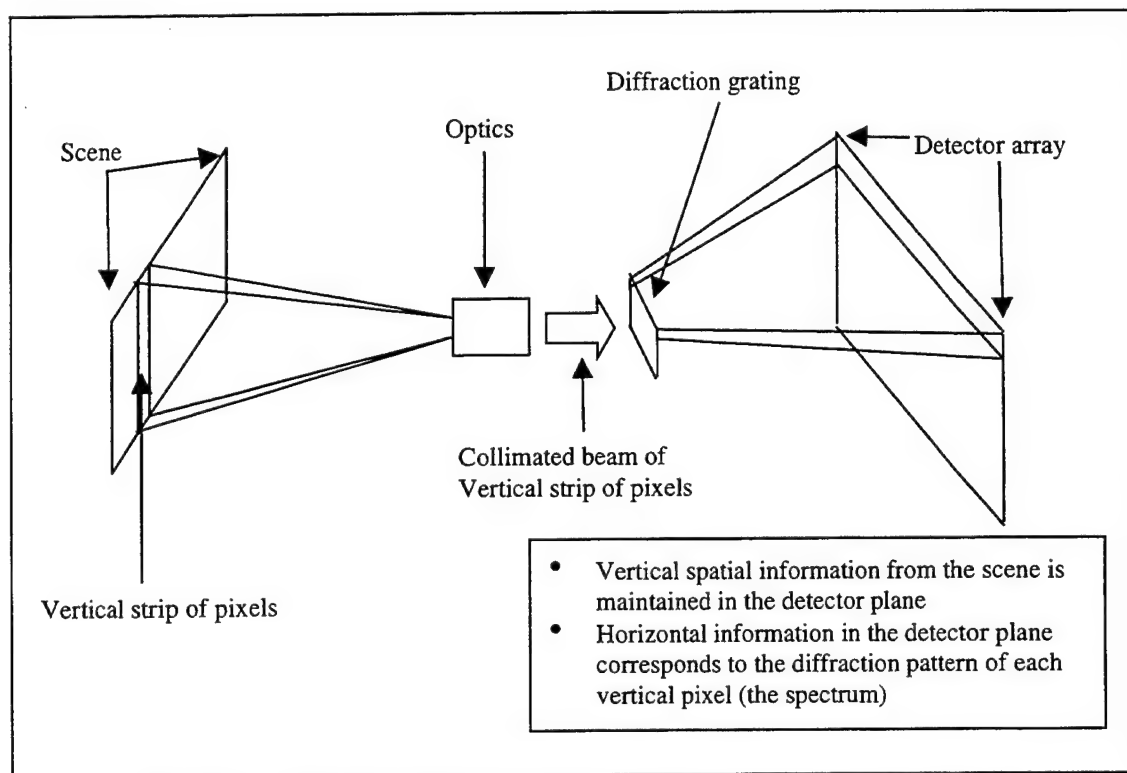


Figure 2.5. Schematic diagram of the mechanics of spectral imaging.

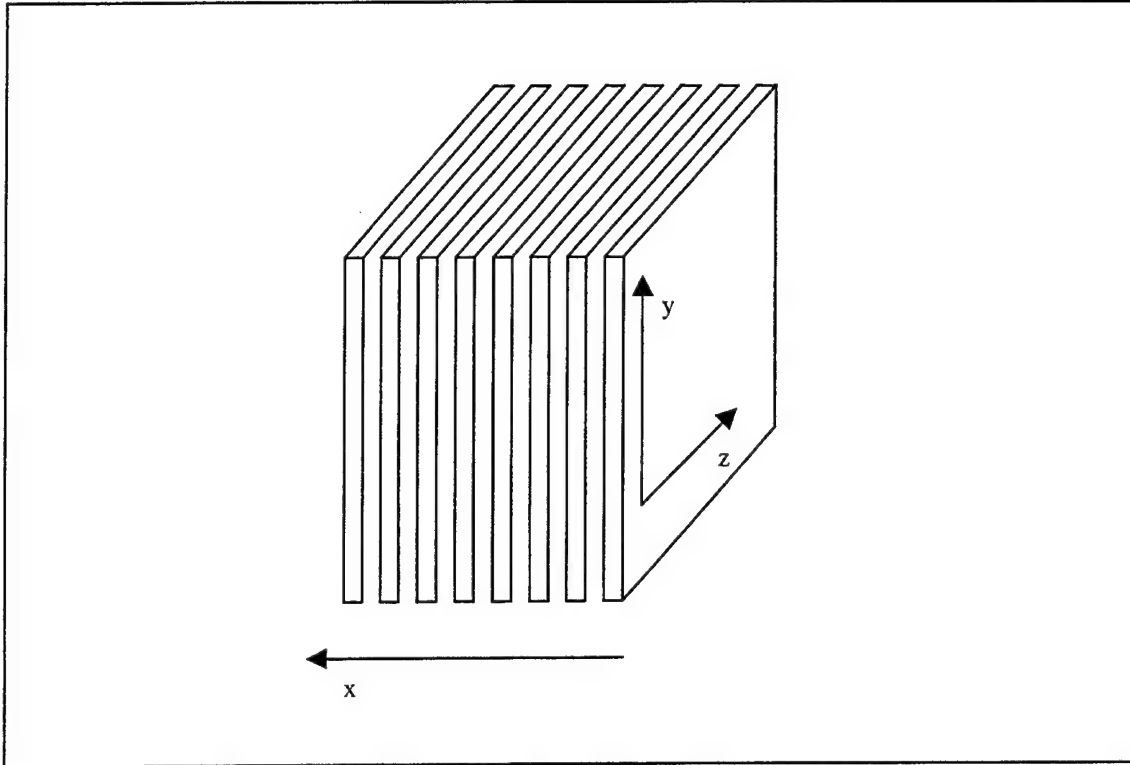


Figure 2.6. Frame stacking to form the spectral cube.

### III. HARDWARE AND SOFTWARE OVERVIEW

LINUS consists of several hardware and software subsystems and modules. The primary hardware subsystems are the passive optics (telescope and spectrometer), the active optomechanical scanner, the camera and the host computer. The interconnected architecture of these subsystems is schematically shown in Figure 3.1.

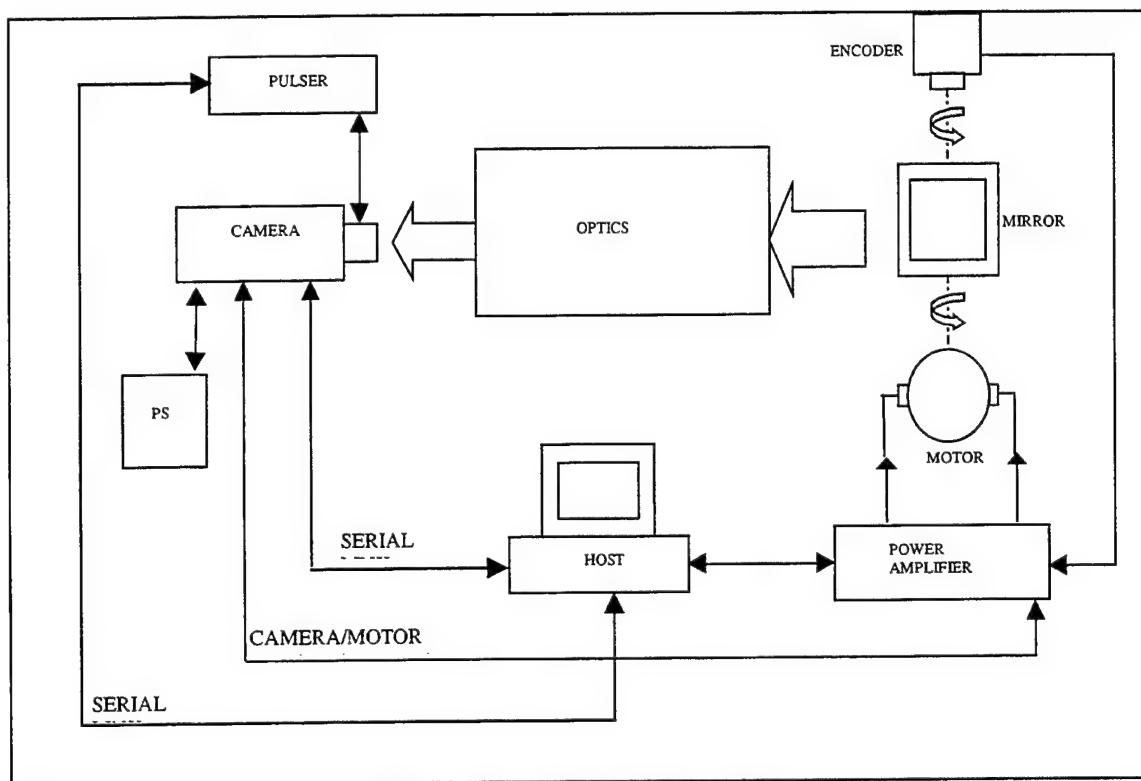


Figure 3.1. LINUS architecture.

At the center of the system and acting as the main processing, synchronizing and control unit is a host computer. The computer oversees all other components of the system. Optomechanical scanning of the scene is achieved by a plane mirror that is rotated about a vertical axis by a servo motor and encoder unit, which in turn is

controlled by a dedicated board installed in the host computer. The mirror mounted in front of the telescope, sequentially steers the scene image across the vertical input slit of the spectrometer. This captured light is directed through the optics which generates the diffraction pattern (spectrum) for each vertical pixel and focuses it on the focal plane of the instrument's dedicated camera. Frames of data captured by the camera are sent for storage and processing to the host computer through a serial link. Once the camera has read out a frame of data, the camera tells the host computer that it has completed the frame. The computer then directs the servo system to point to the next vertical strip in the scene. When the servo has settled at the new position, it informs the host computer, which then triggers the camera to take the next frame of data. This iterative process goes on until the whole scene of interest has been recorded.

The rest of this chapter reviews the general characteristics of the hardware and software that constitute LINUS. For convenience, the system has been divided in the following sub-systems:

- Host computer
- Servo system
- Optics
- Camera system

## **A. HOST COMPUTER**

The host computer is an ICS Advent system composed of a 7490 Series chassis, a 14.1" liquid crystal video display, keyboard and mouse, all specifically ruggedized for field use.

The chassis [8] is a sturdy frame that can be used either on a bench top or mounted in a standard 19" rack, as shown in Figure 3.2. The front panel has a locking door to prevent unauthorized access and to protect the unit during transit. The only visible portion of the front panel consists of LED indicators that give the status of power supply voltages, proper fan operation, hard drives and operating temperature. Opening the front panel door gives access to the chassis power switch and disk drives. Internally, the chassis is fitted with a thirteen-slot backplane [9] as shown in Figure 3.3, and a power supply. The backplane can accommodate one CPU board, 6 ISA cards and 6 PCI cards. The CPU board chosen for the LINUS application is a single board computer of the SB686BX Series [10], and is based on an Intel Pentium processor. The LCD display and keyboard shown in Figure 3.4 are also housed in rugged mounts to allow for easy transport and field operations. Both the display and keyboard are also 19" rack compatible.

At the time of this writing, the computer operates under control of Microsoft Windows NT 4.0 operating system. It has all the conventional standard input and output devices, plus for a 1 gigabyte Jaz drive. This high capacity drive was included because imaging applications are data intensive, requiring a great deal of data storage capability.

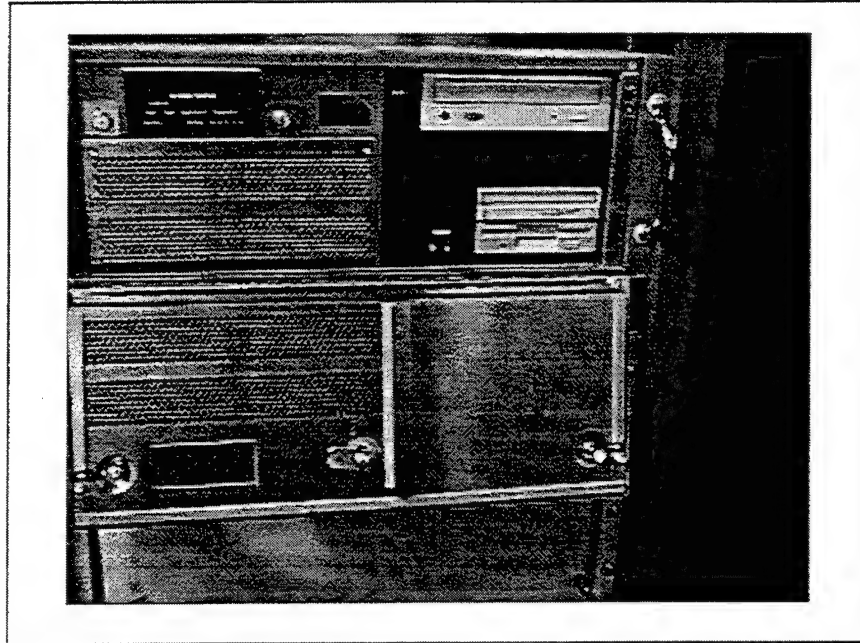


Figure 3.2. Computer chassis.

## B. CAMERA

The camera chosen for the application is a Princeton Instruments Intensified Pentamax System [11]. It consists of an ultraviolet intensified CCD camera, power supply, a PG-200 pulser with the MCP-100 high voltage power supply option, and a high speed serial link board. The camera is shown in Figure 3.5 and the power supply in Figure 3.6.

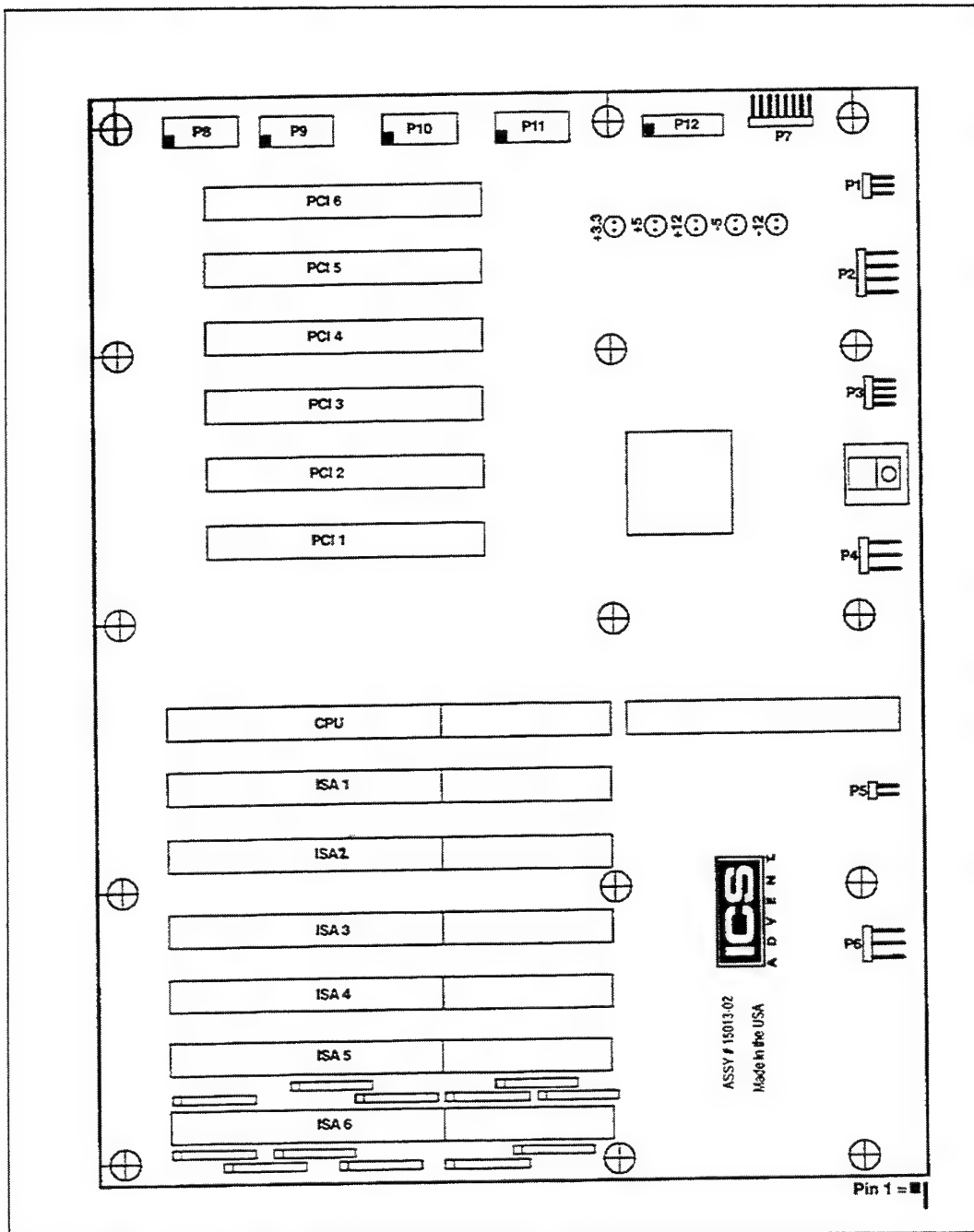


Figure 3.3. Computer backplane [9], showing card slot locations.



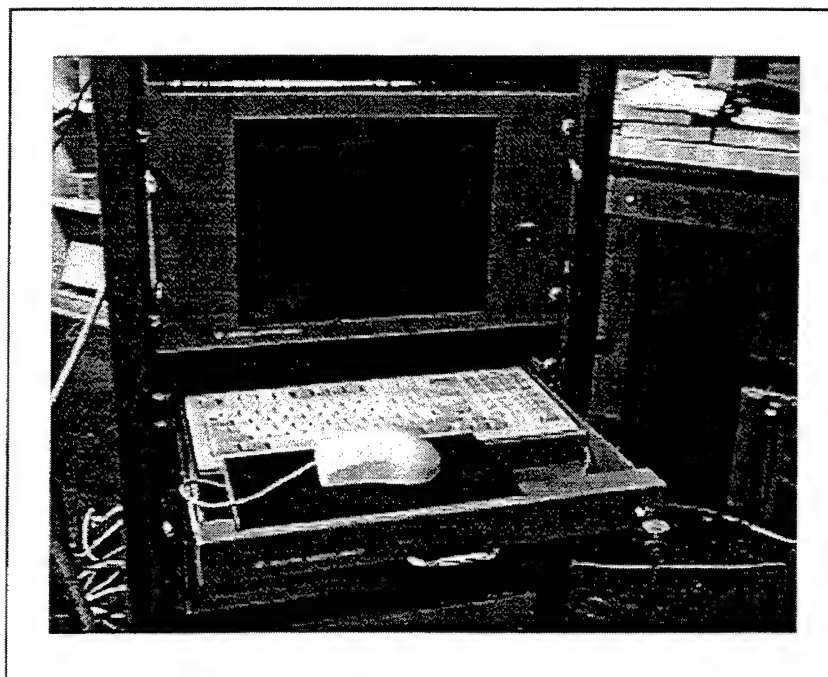


Figure 3.4. LCD display, keyboard and mouse.

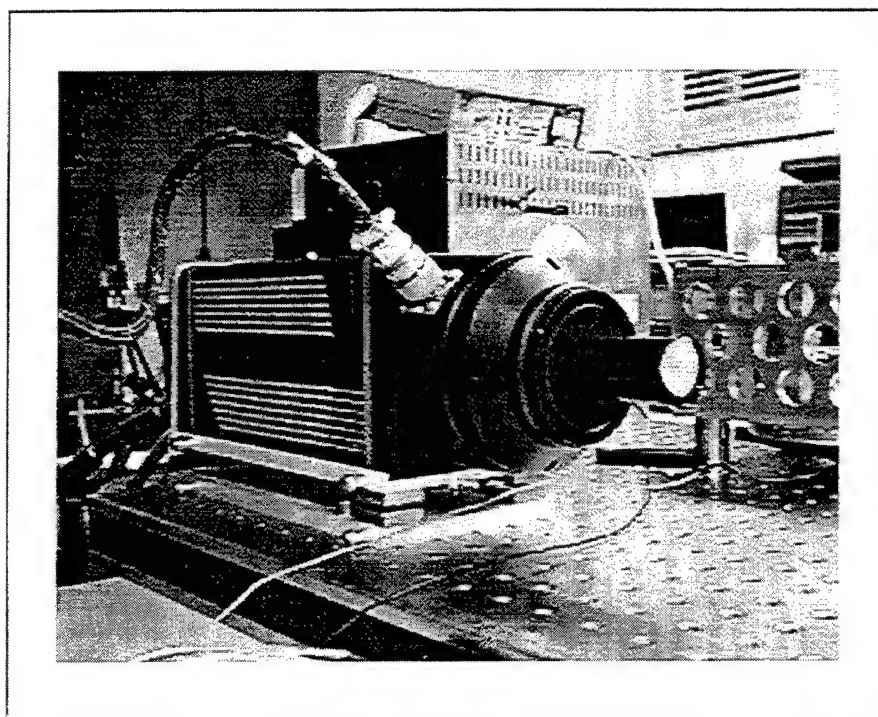


Figure 3.5. Pentamax camera with its integrated image intensifier.



Figure 3.6. Pentamax power supply and temperature controller.

At the front end of the camera is an integrated, ultraviolet enhanced microchannel plate (MCP) image intensifier. The output of the intensifier is optically connected to a 512x512 charge coupled device (CCD) detector array via a tapered fiber optic bundle. The camera has a built-in thermoelectric refrigeration unit. The camera interfaces to the host computer through a high speed serial link (RS-232). Data transfer to computer memory is achieved by a dedicated PCI buffer board. Camera control and data acquisition are accomplished by the host computer. Power to the camera is provided by a separate power supply which also incorporates a closed-loop temperature monitoring and

control unit for the CCD refrigerator. The camera is able to adapt to several timing and readout modes, making it very flexible. Trigger and high voltage pulses for the camera and its MCP image intensifier are provided by the PG-200 pulser [12] shown in Figure 3.7. Even though the pulser is a stand alone unit, it can also function under computer control and is interfaced through one of the general service serial ports (COM2). This provides for ease of operation, because configuring the pulser through the control software shipped with the system is easier than through the front panel.



Figure 3.7. PG-200 pulser.

### C. SERVO SYSTEM

The servo is a closed-loop angular position control system that points the image scanning mirror to any desired heading. It consists of a permanent magnet DC motor, a digital incremental encoder, a power amplifier, and a motion controller interface card.

The control element is a National Instruments Flexmotion 6C motion card [13]. It is a fully programmable board that interfaces to the host computer via the PCI bus. The board has high performance capabilities resulting from a dual-processor architecture. It combines a Motorola MC68331 real-time 32-bit CPU with an Analog Devices ADSP 2111 digital signal processor and custom field programmable gate arrays. The embedded real-time CPU integrates all the functions of the card including host-controller communications, motion command processing, onboard program execution, error handling, etc. One of the most powerful features incorporated in Flexmotion is the capability of executing onboard programs independently of the host computer. It can run up to 10 simultaneous motion programs in a real-time preemptive multitasking environment. This allows operation of highly synchronized applications that require minimum latency between events. The main virtue of implementing a motion application as onboard programs is the load taken off the host computer, which normally is not well suited for real-time applications. The Flexmotion card has all the input and output resources to control up to six independent motion axes including, feedback devices, limit switches and several general purpose input/output signals. The command output provided by the board is an industry-standard  $\pm 10$  volt signal.

The DC servo motor chosen for LINUS is a Kollmorgen Motion Technologies Group high torque low-inertia "pancake"-type unit, model 12FS. It is driven by the

Flexmotion board through a National Instruments nuDrive [14] power amplifier, as shown in Figure 3.7 above the PG-200 pulser. Besides being a general-purpose DC power amplifier, the nuDrive also serves as an interface between the Flexmotion board and various control signals. nuDrive also converts the  $\pm 10$  volt command signal to a 20 KHz pulse-width-modulation signal, providing very precise drive for the motor.

The position feedback for the servo is provided by an ultra-fine precision rotary incremental digital encoder. It is a Gurley Precision Instruments device, model R137. The encoder has a resolution of 144,000 counts per revolution, a value that corresponds to a per-pulse angular resolution of 43.6 micro-radians or 9 arc seconds. It provides a quadrature RS-422 differential signal to the Flexmotion board to close the control loop, and it also provides an index signal in order to be able to bring the servo to a known position upon system power-up.

The scanner mirror assembly shown in Figure 3.8 houses two of the four components of the servo. The assembly is composed of a cage that supports the electric motor (shown on the bottom), the encoder (shown at the top), and the mirror housing (in the center). Special consideration was taken in the design of the mirror housing so that it has low inertia and is properly balanced to not generate disturbing torques when the instrument is tilted. The motor shaft is attached directly to the mirror housing, while the encoder is linked to the shaft by a flexible coupling to absorb minor misalignment and avoid spurious torques which could damage the encoder.

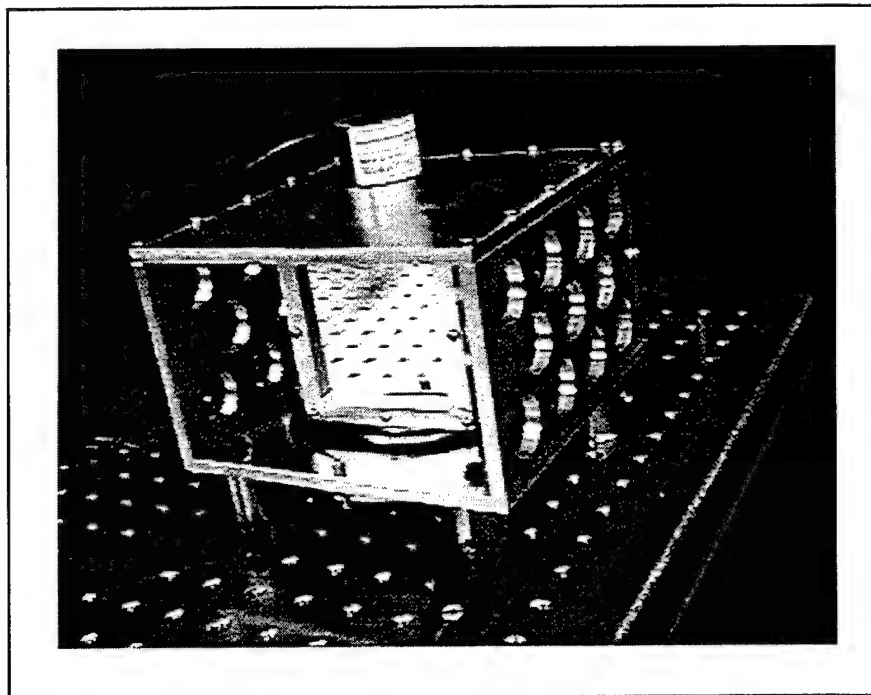


Figure 3.8. The mirror optomechanical scanner, consisting of supporting cage, servo motor, rotary encoder, mirror housing and mirror.

#### D. OPTICS

LINUS's optical layout is shown in Figure 3.9. At the front end is the scanner mirror which is operated by the servo system. The radiation reflected by the mirror is filtered so that only the spectral bandwidth of interest goes into the system. Following the filter is the primary telescope objective, which focuses the radiation onto the vertical slit input aperture. After the slit, a collimating lens sends the light to a reflective plane diffraction grating. The light bouncing off the diffraction grating is then captured by the camera objective which focuses it onto the input plane of the camera's image intensifier.

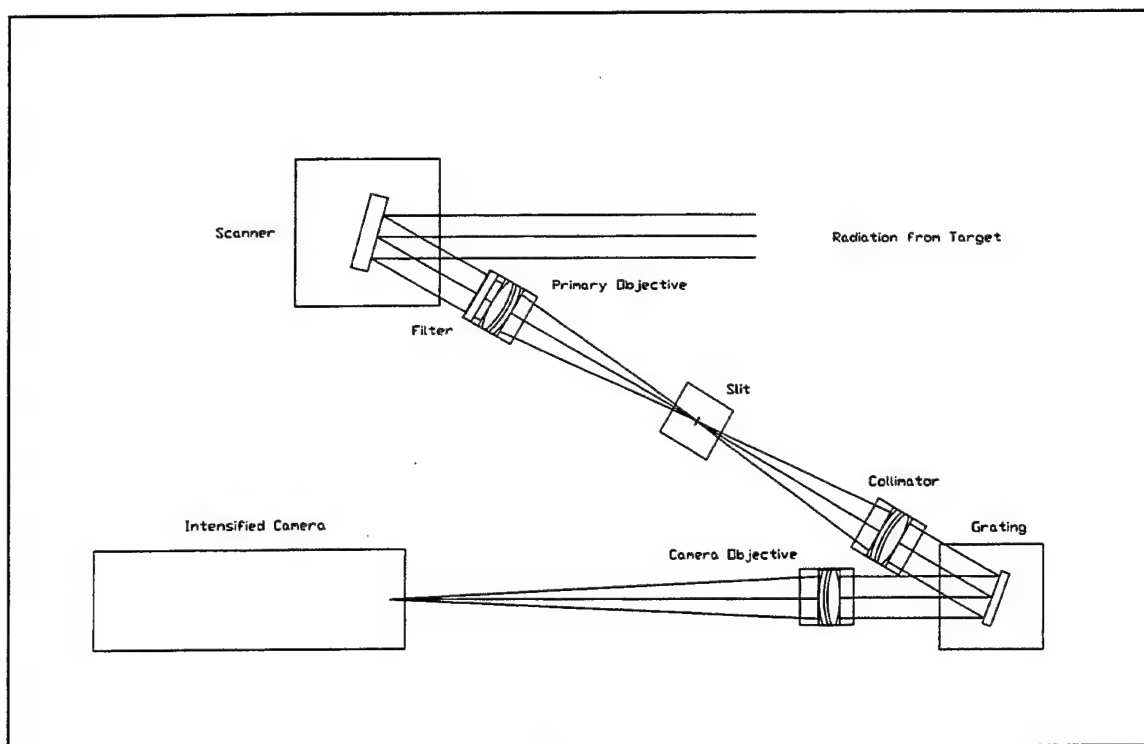


Figure 3.9. The optical layout.

## E. SOFTWARE

The software development tool chosen for LINUS is a programming environment called LabView, by National Instruments. LabView [15] is much like any modern programming environment, but it is different in one important respect. It is based on the graphical programming language G [16]. All existing high level languages, in general, are text-based and some are supplemented by visual aids, but they remain text-based. G is a truly graphical language that really speeds up application development. The Pentamax camera and Flexmotion board come with LabView libraries that makes building new applications rather simple.

Even though programming in G is very simple, it is not a straightforward process to go from structured text-based programming languages to G. It requires a thorough

study of several month's duration, executing tutorials, reading manuals and hands-on practice in order to understand the underlying principles involved, and how they differ from those of normal programming languages. But the reward is gratifying. Powerful applications with instrument-like graphical user interfaces can be built in relatively short time. Examples of the G software for LINUS are given in Appendix B.



THIS PAGE INTENTIONALLY LEFT BLANK

## **IV. THE SERVO-SYSTEM**

The image scanner servo system is one of the crucial parts of the whole system, and its development formed the core of this thesis project. It is electromechanical in nature, and its purpose is to accurately rotate the mirror in well-defined, small incremented steps to scan the field of view of the instrument across the entrance slit. The mechanical accuracy and stability of the servo can limit the quality of the imaging if it does not perform well.

This chapter reviews the integration of the components that constitute the servo-system as described in chapter III, the driving of the system, and the servo tuning.

### **A. SERVO SYSTEM BASICS**

The purpose of the servo system is to provide precise and accurate control of the angular position of the image scanning mirror. Hence, this type of servo is called an angular positioning servo. Other types of generic families of servos exist, including linear positioning systems, velocity control systems, and so forth.

All servo systems share the common trait of employing feedback loops to dynamically control the mechanical parameters of interest. If the controlled parameter is perturbed in some way, the servo acts to inject an opposing signal that corrects the disturbance. The primary agent of this operation is a negative feedback loop. Figure 4.1 shows a generic diagram for such a loop; more complex examples may be found in reference [17].

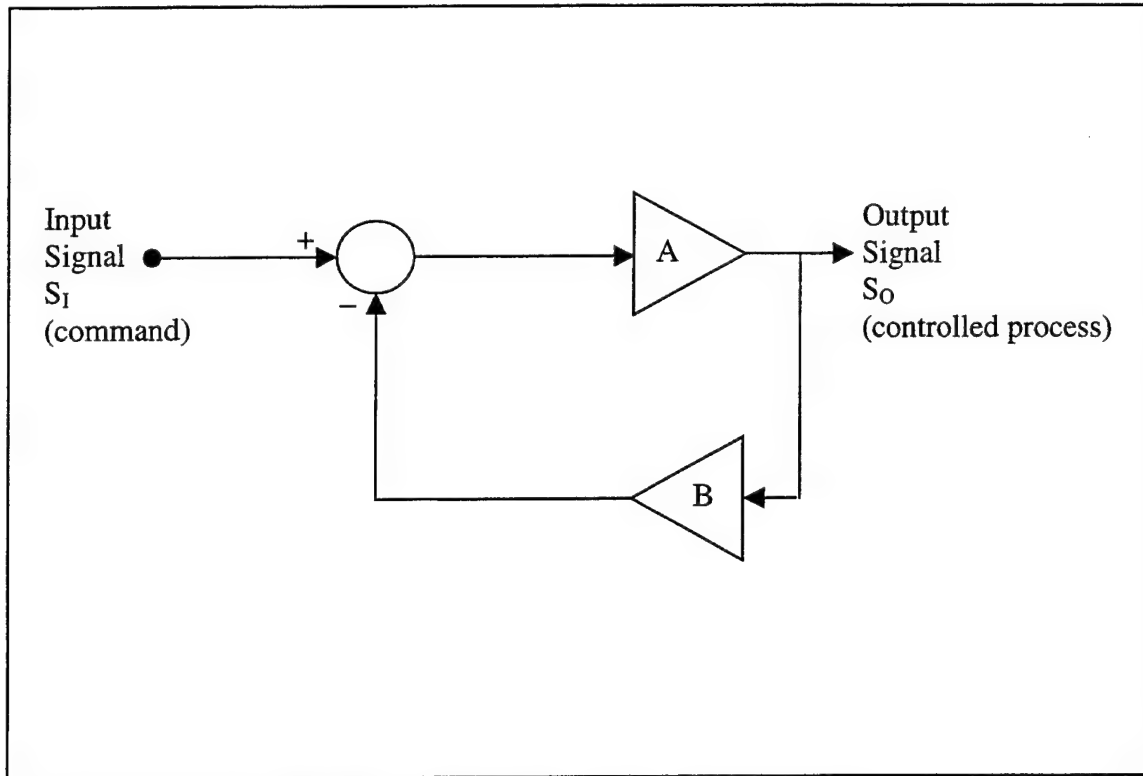


Figure 4.1 Feedback loop of a control system.

The circular symbol denotes a differencing unit whose output is equal to the difference of its inputs, as shown. Unit 'A' is an active element, usually consisting of an amplifier-filter device whose output is A times its input. The parameter A is usually frequency dependent and is complex-valued to incorporate any phase shifts. Unit 'B' is a similar device whose output is B times its input. A and B are called the transfer functions of the two devices.

Looking at the diagram, we see that the input to 'A' is  $S_1 - BS_0$ . Therefore,

$$S_0 = A(S_1 - BS_0), \quad (4.1)$$

so that

$$S_o = \frac{AS_I}{1 + AB}. \quad (4.2)$$

The ratio  $S_o/S_I$  is called the closed-loop transfer function of the system, and is given by

$$\frac{A}{1 + AB}. \quad (4.3)$$

It is clear that  $S_o$  is a well-behaved function of  $S_I$  provided that  $AB \neq 1$ .

For the LINUS scanning system, the input control signal is a mirror-rotation signal generated by the control computer. The output signal is a set of quadrature angular displacement pulses from a fine precision rotary encoder. The encoder is driven by the same DC motor which turns the scanning mirror, under control of a power amplifier ('A'). Once the mechanical and electrical components of such a system are constructed, the task becomes one of manipulating the shapes of the complex transfer functions  $A(\omega)$  and  $B(\omega)$  to achieve the classical degree of stability and control performance. This is known in control systems terminology as "tuning the servo."

The mechanical portions of the scanner, including the superstructure design, motor and encoder specifications, are given in Appendix A.

## **B. INTERFACING THE COMPONENTS**

The first step in the process of integrating the servo system was the installation of the National Instruments Flexmotion card in the host computer. Before installing the card, it was necessary to configure jumpers and place appropriate resistor networks for compatibility with the other electronic components in the system.

The Flexmotion board provides the means to optically isolate the motion I/O signals from the I/O devices to reduce noise sensitivity. This feature allows for two options regarding the powering of I/O signals. If no optical isolation is decided for the application, the I/O signals are fed from the computer's internal +5V power supply. If optical isolation is required, an external power supply must be provided in the range +5V to +24V. To implement one of these alternatives the jumper JP2 and resistor networks RP3 and RP10, shown in Figure 4.2, must be correctly set on the board. In order to facilitate the initial work in the comparatively low-noise lab environment, it was decided to use the non-isolated option. The jumper JP2 was configured for internal +5 V, so 470  $\Omega$  resistor networks were installed in RP3 and RP10 [13].

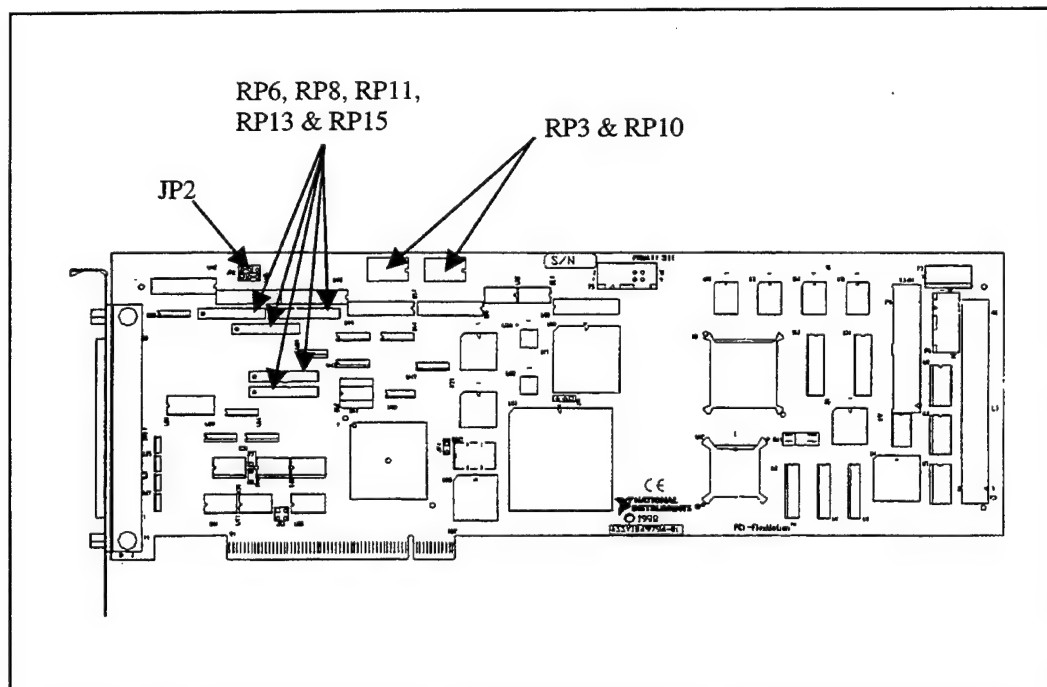


Figure 4.2. Adjustable jumper and resistor networks on the Flexmotion board.

It was also necessary to install the proper resistor networks for encoder termination (impedance matching) on the board. This adjustment optimizes encoder signal performance. The value of the resistor networks is dependent upon two factors: the maximum expected frequency of the encoder input signals, and the nature of the encoder line driver (differential or single ended). Because the encoder selected for the application is of the differential type, and it works at less than 1 MHz, termination networks RP6, RP8, RP11, RP13, and RP15 were set at 1.5 k $\Omega$  and 3.3 k $\Omega$  correspondingly [13].

The Flexmotion board was installed in slot PCI-3 in the host computer backplane. Input and output signals are routed from the board to the power amplifier through a 100 pin connector. The power amplifier also serves as an interface where all input/output signals are physically connected to the respective motion devices.

The power amplifier drives the servo motor through balanced, floating positive and negative leads that provide a 48 V signal, pulse-width modulated (PWM) at 20 KHz. The motor power terminal block in the rear panel of the National Instruments nuDrive module is connected as shown in Figure 4.3. The digital encoder is connected to the corresponding terminal block on the amplifier input connector, as shown in Figure 4.4. The encoder +5 V power supply voltage is also provided by the amplifier. The other signals are the quadrature differential encoder pulses labeled A and B, the index differential signal, and the encoder signal ground.

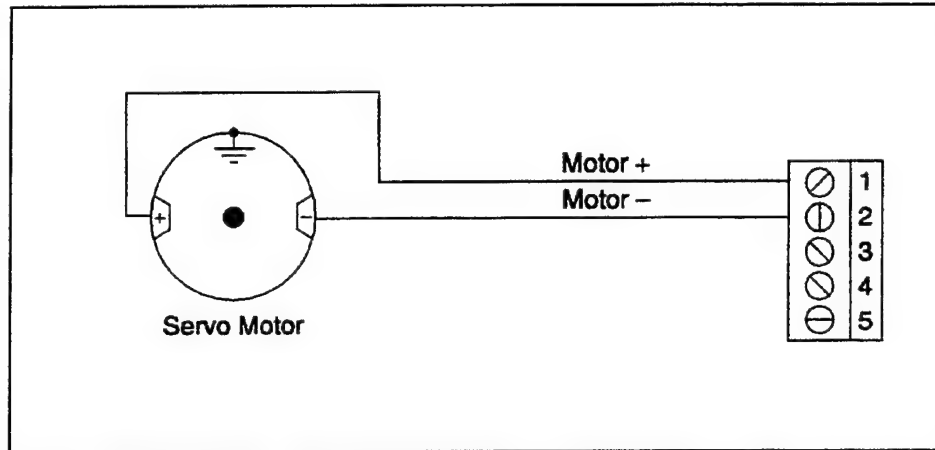


Figure 4.3. Motor connection to the nuDrive [14].

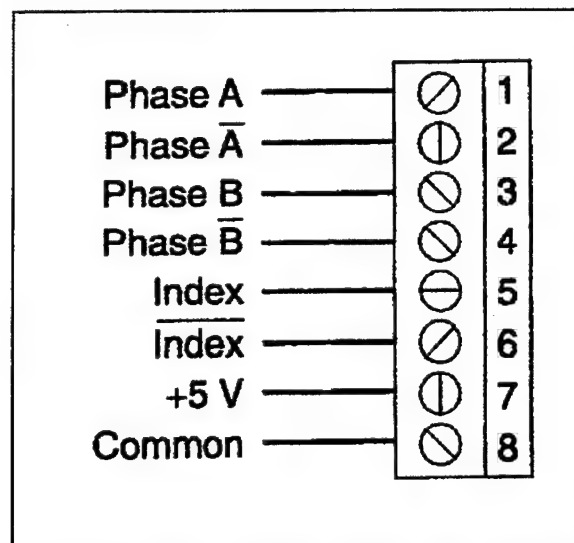


Figure 4.4. Encoder terminal block in the nuDrive [14].

### C. DRIVING THE LOAD

The first attempt to drive the servo motor was done with a manufacturer-supplied test application shipped with the board. The application is called Flexmotion Commander, and it provides options for board configuration and simple motion tests. Once the system was initially configured, it did not accept the full number of 144,000 counts per revolution generated by the encoder. After further testing, it was determined

that version 4.0 of the Flexmotion firmware only accepts 16 bit words in its counting registers, limiting its capability to 65535 counts per revolution. This issue was resolved by updating the Flexmotion firmware and software to version 5.0, which accepts up to 32 bit words.

The most fundamental servo task is to maintain the scanning mirror fixed and stationary. This was tried with success, but it was discovered that the servo motor was dissipating a great deal of heat, even though it wasn't actually driving a rotating load at the time. Ohmic heating would be expected with the motor rotating, because the rating of the motor is 21.6 V and the output voltage of the nuDrive is 48 V. However, heating of the stationary motor remained a puzzling problem for a time, until the issue was solved using the online knowledge base at National Instruments [18]. The overheating of the motor occurs because the drive is PWM. The high frequency sharp discontinuities in the driving voltage signal, together with the low intrinsic inductance of the motor cause high power dissipation due to large current spikes, even under ostensibly quiescent conditions. These large current spikes can be controlled by adding a balanced set of inductors to the motor leads as shown in Figure 4.5.

The appropriate inductor value can be determined from the following equation [18]:

$$L = \frac{V}{f} \sqrt{\frac{R}{P}} \text{ mH}, \quad (4.4)$$



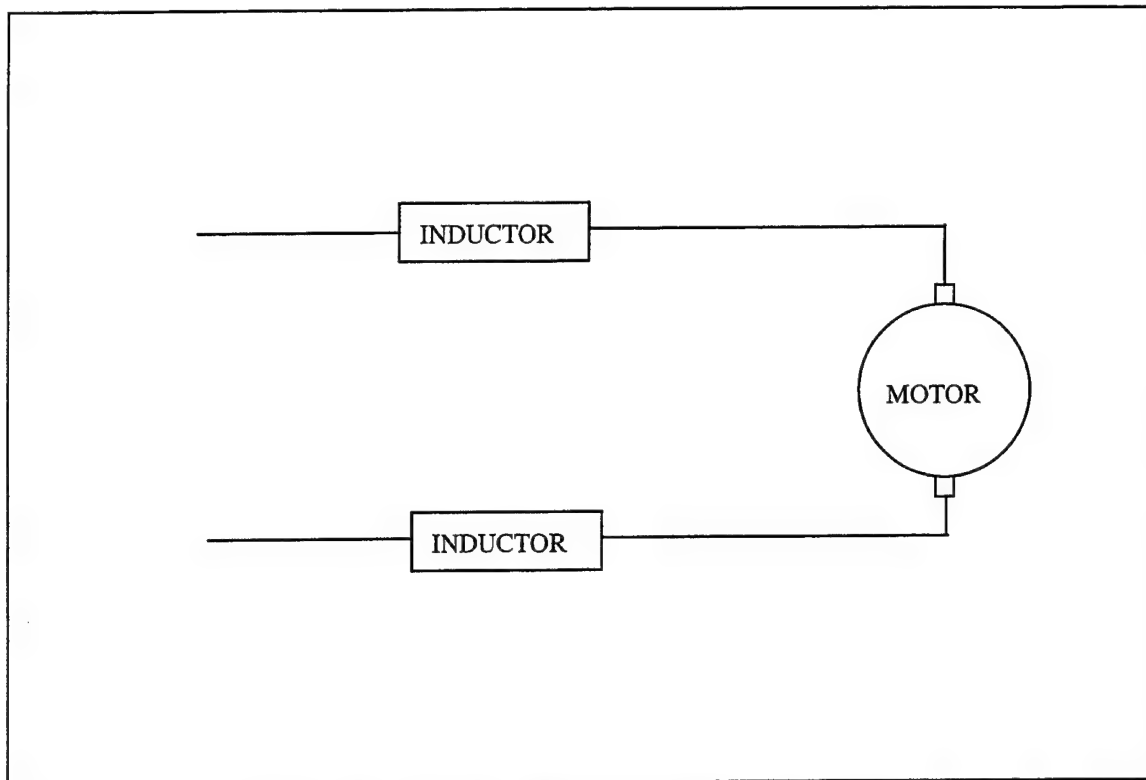


Figure 4.5. Control of heat dissipation in the motor.

where  $V$  is the power amplifier output voltage,  $f$  is the PWM frequency,  $R$  is the motor's DC input resistance, and  $P$  the maximum allowed power dissipation for the motor. It was estimated that 10 W is a reasonable power dissipation for the motor. The calculated value for the inductance is approximately 1 mH. Because the inductance must be installed as a balanced set, two 0.5 mH inductors are used. They are rated for 10 amperes, the peak current output of the power amplifier. Even though the 10 W dissipation was only an initial estimate, it turned out to be an adequate value, and the quiescent motor heating problem was solved.

Once the heat dissipation problem was solved, the next step was to experiment with the system in different modes to acquire familiarity with the hardware and software.

The servo was made to rotate at constant speed in both clockwise and counterclockwise directions, and to execute steps of different amplitude using the Measurement Automation utility that replaces the Flexmotion Commander for version 5.0 of the software.

The initial software configuration was found to be very limiting and made some iterative testing processes very tedious. This is where LabView [15] and the Flexmotion VI Library came in handy. Two simple programs were developed to accommodate the laboratory testing needs of LINUS. Both are listed and explained in Appendix B. "Linus Initialization.vi" was developed to initialize the board to the parameters that are required for LINUS's operation. This program must be run every time the system is turned on and when the state is unknown. "Linus Stepping Program.vi" is designed to make the servo move a number of steps of certain amplitude and in a direction defined by the operator.

#### **D. TUNING THE SERVO**

The tuning of a closed-loop servo system basically entails the careful tailoring of the closed-loop transfer function

$$\frac{A(\omega)}{1 + A(\omega)B(\omega)} \quad (4.5)$$

for optimum behavior across the frequency band in which the servo is to be operated. Eq. 4.5 is the same as Eq. 4.3 (the closed-loop transfer function), except that parameters A and B are now shown as explicit functions of angular frequency  $\omega$ . While seemingly trivial in concept, this tuning operation can be quite complicated in practice. Many characteristics of the complete system must be taken into consideration. For instance,

each mechanical member of the system, such as shafts, struts, plates, etc. will have a characteristic set of vibrational resonant frequencies. As is well known, any mechanical system driven at a frequency near a resonance will be highly susceptible to large amplitude oscillations, unless proper damping is included. Furthermore, the response of a system near resonance exhibits pronounced phase shifts as a function of frequency. Great care must be exercised in a high-gain servo system, lest these phase shifts change the negative feedback transfer function [Eq. 4.5] into a positive feedback condition, with  $A(\omega)B(\omega) \rightarrow -1$ , thereby leading to uncontrolled oscillation. Therefore, both the mechanical design of the components and the establishment of  $A(\omega)$  and  $B(\omega)$  must be handled carefully.

For example, the mechanical drawings for the components of the scanner show that many members have had a number of staggered holes drilled through them (see Appendix A). These holes serve three purposes. First, they lower the weight of the device. Second, they provide for adequate air flow and thermal equilibration. Third, and most importantly, they raise the resonant frequencies of the vibrational normal modes of the components above the frequency bandwidth associated with normal servo operation.

Additional damping and filtering of the closed-loop transfer function may be done by altering the gain and phase characteristics of  $A(\omega)$  and  $B(\omega)$  as functions of frequency. That is, the filtering of the closed-loop transfer function is adapted, or tuned, to produce desired behavior. Viewed from a frequency domain perspective, this means that  $A(\omega)$  and  $B(\omega)$  have their gain magnitude and phase responses modified so that singularities (poles) in the closed-loop response are removed from the operating

passband. For a sinusoidal input at some frequency  $\omega$ , the easiest way to alter a circuit's response is to add in some portion of both the signal's time derivative and time integral, which provide phase shifts of  $\pm\pi/2$ . Hence, this form of filter refinement is called proportional-integral-derivative (PID) control. It is a very powerful and effective means of configuring closed-loop transfer functions.

The Flexmotion's hardware and firmware system implements PID by means of digital control algorithms. The Flexmotion VI Library provides a program called "Servo Tuning.vi" that makes this task relatively simple.

Because of the stepping nature of the mirror scanning application in LINUS, a time domain step-response technique was chosen for tuning in this instance. Sharp stepping transients consist of a broad frequency range of behavior, so careful broadband servo response is needed. Details of the procedure and considerations for tuning the servo are described in Appendix C.

THIS PAGE INTENTIONALLY LEFT BLANK

## V. TEST RESULTS

This chapter summarizes the results of a number of performance tests of the LINUS image scanner servo system. Both static and dynamic responses are characterized, as well as overall scanner stability and pointing accuracy.

### A. DYNAMIC STEPPING TESTS

The dynamic performance of the servo system for various stepping configurations is summarized in Figures 5.1 and 5.2. The term "step" here means one complete encoder count, or an angle of  $2\pi/144,000$  radians ( $2.5 \times 10^{-3}$  degree = 9 seconds of arc). The positioning error is in encoder counts, or increments of 9 seconds of arc.

The graph in Figure 5.1 shows error versus time in milliseconds. Analyzing the data, it can be seen that the maximum overshoot of the system is close to 25 counts, less than 5% of the 1000 count step, which is considered a good criterion in Control Engineering. The tuning was aimed to yield the least rise time possible, obtaining a final value of less than 15 ms. The criterion for settling time was defined to be when the error remains within  $\pm 1$  count of the final position, and the value obtained is approximately 30 ms.

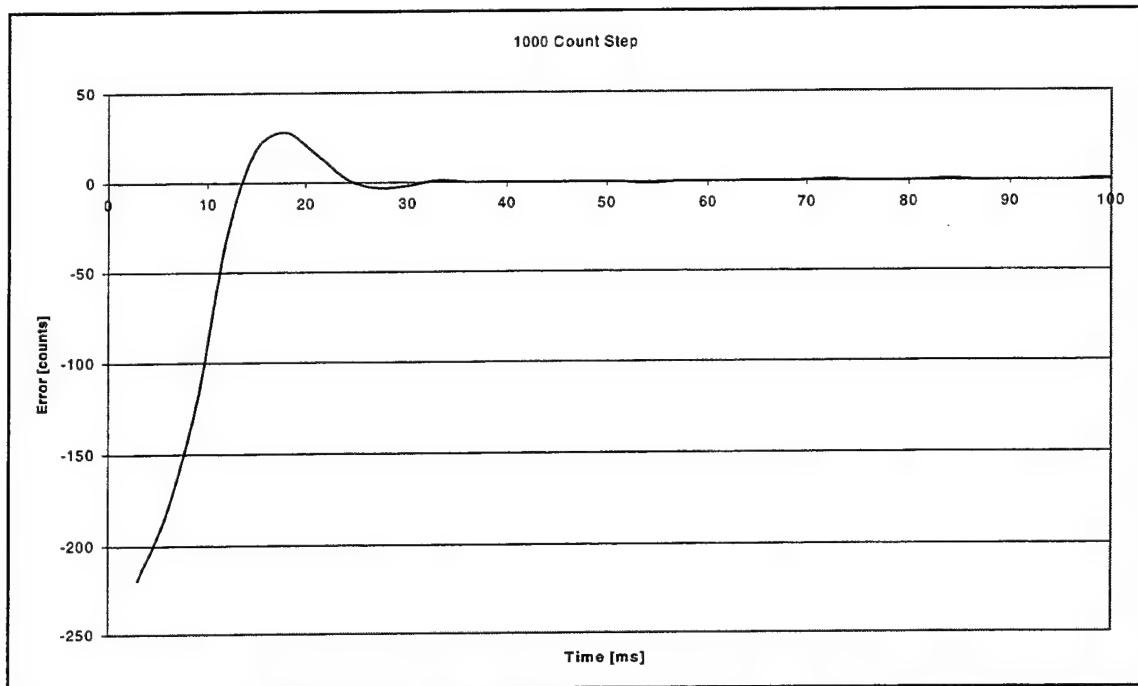


Figure 5.1. Step response for a 1000 count step.

Figure 5.2 plots a 100 count step with the same PID parameter values. The observed trend is improvement in all performance measures. Maximum overshoot is approximately 6 counts while rise time is around 5 ms. Settling time improves to a value better than 15 ms. This trend indicates that for smaller steps and same PID parameters, the servo performs better, and that is why tuning was done for a 1000 count step.

Tuning was performed with the mirror frame only, because the mirror was on order when the process took place. Once the mirror arrived, it was installed and the response to a 1000 count step is shown in Figure 5.3.

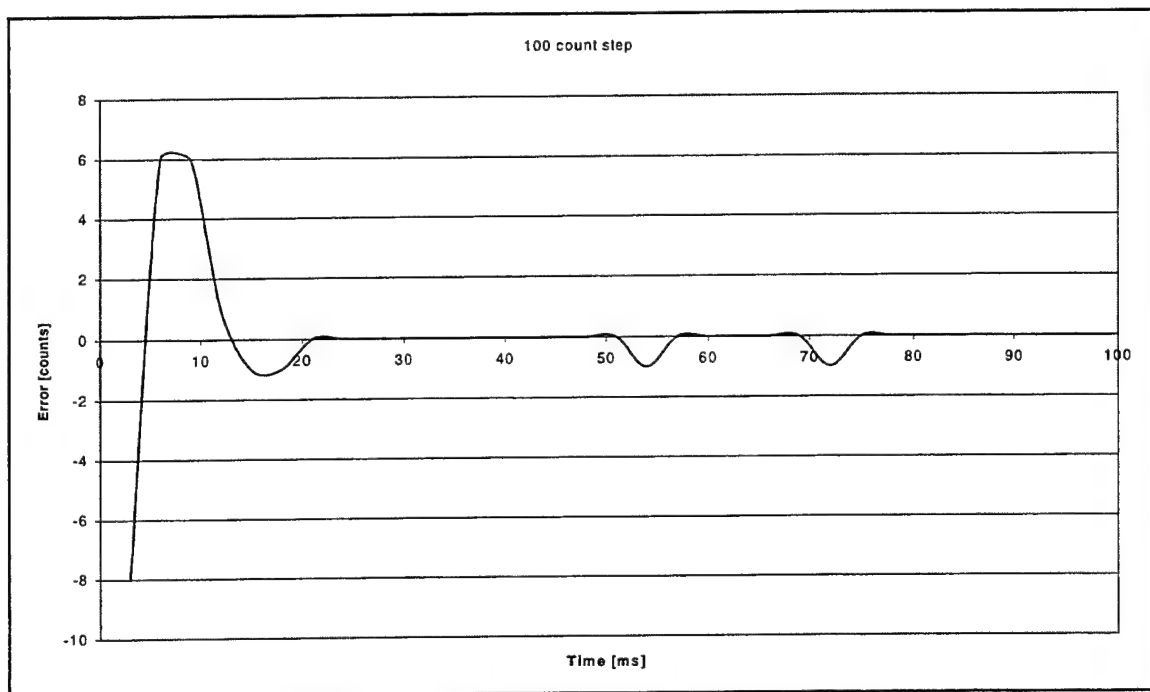


Figure 5.2. Step response for a 100 count step.

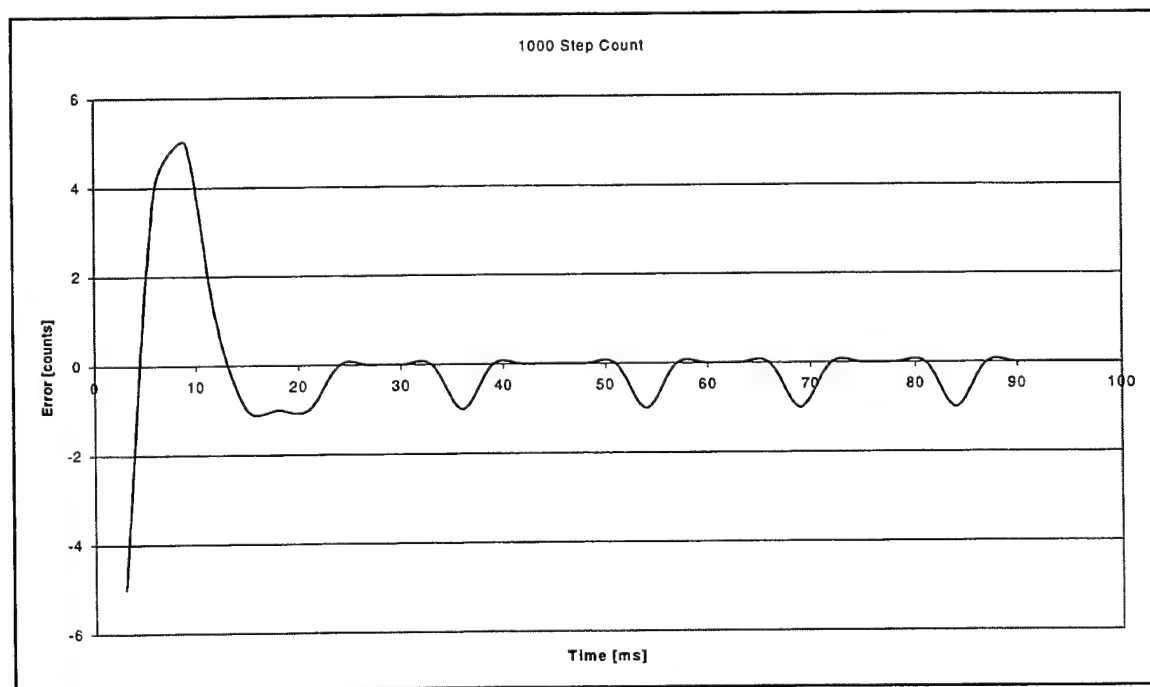


Figure 5.3 Step response with mirror.



The apparent  $\pm 1$  count oscillation observed in all plots is expected because the servo cannot be completely static. At this point in the design it is not possible to determine how this will limit the imaging quality of the system. If this becomes an issue, it will be necessary to change the digital position encoder for one with better resolution.

## **B. STATIC STABILITY TEST**

Tests were conducted to determine if the positioning was stable or unstable. The setup of the test is shown in Figure 5.4. A solid state laser was shone on to the scanning mirror through a narrow slit, in order to make the beam narrow. This beam was sensed by an amplified photo detector, and the output signal coupled to a spectrum analyzer. Without disturbance, the servo is positioned and the light falling on the detector yields a DC output, hence the spectrum only has a dominant component near 0 frequency as shown in Figure 5.5. Smaller frequency components are also visible, and correspond to the periodic  $\pm 1$  count error evident in Figure 5.3.

The disturbance to the servo was generated by banging the table where the servo was mounted. Figure 5.6 shows the frequency spectrum of the response of the servo at an instant after the disturbance. Assuming that the sharp perturbing mechanical impulse was approximately a narrow rectangular function of time, the frequency response of the servo should roll off as  $1/f$  or faster (i.e. as the Fourier power spectrum of a rectangular pulse). Figure 5.6 shows that response, indicating good stability of the system to external mechanical perturbations.

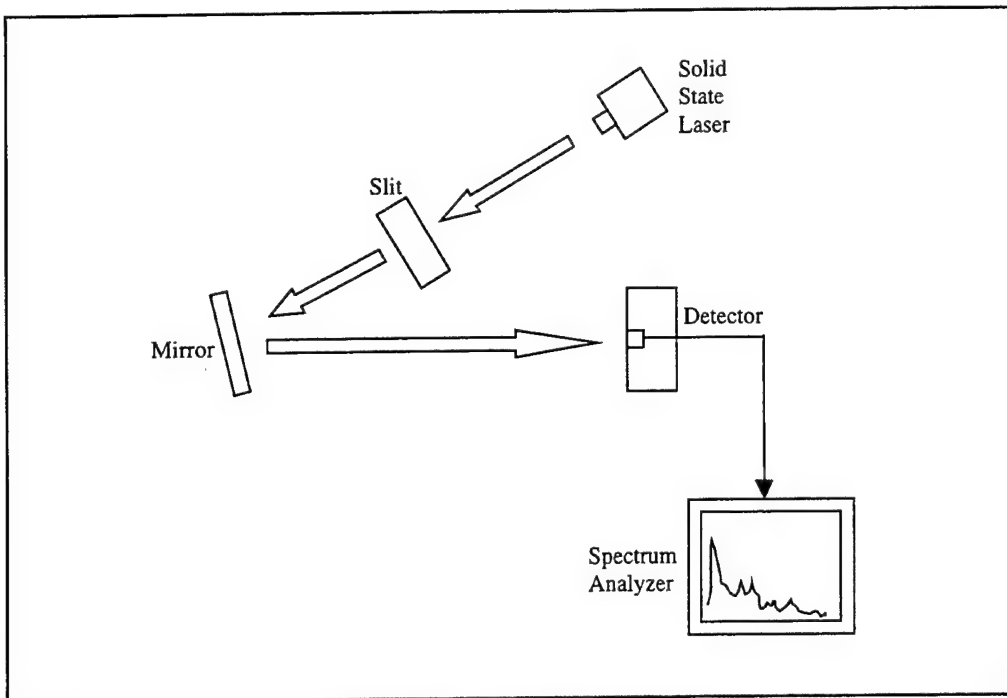


Figure 5.4. Stability test setup.

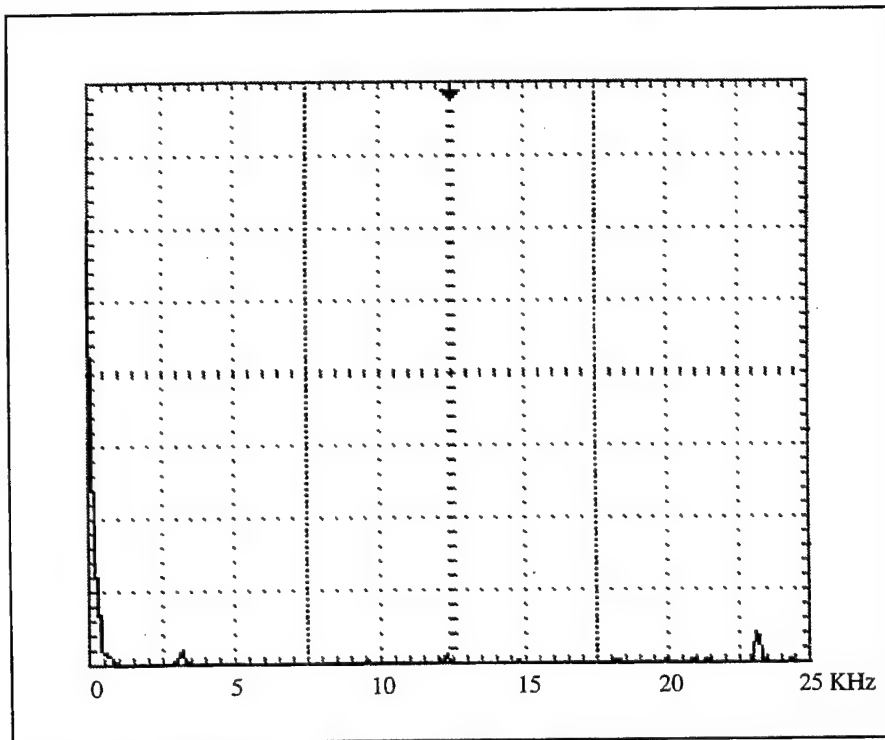


Figure 5.5. Spectrum plot without disturbance.

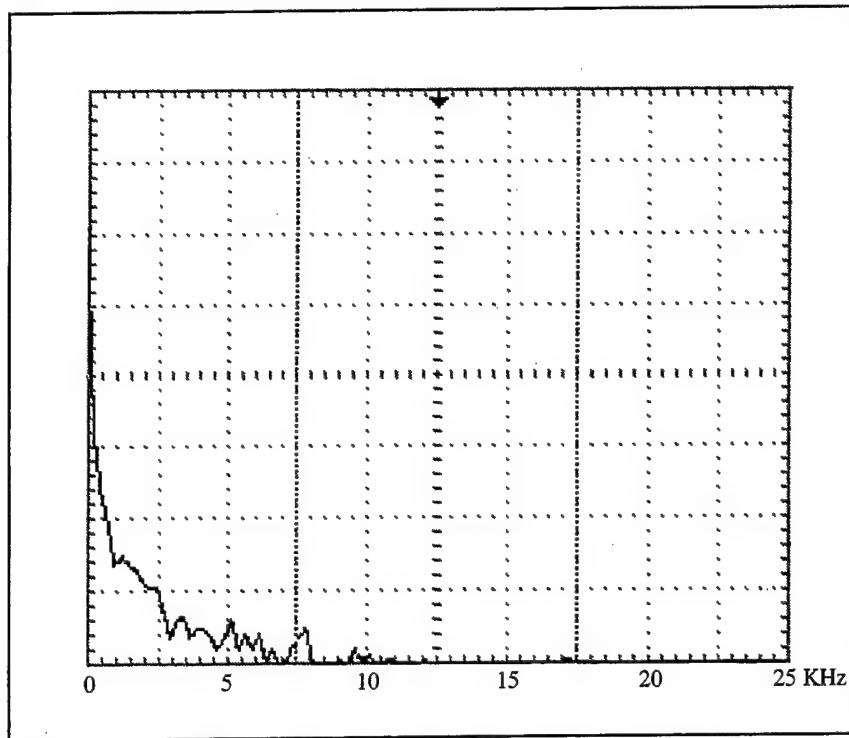


Figure 5.6. Spectrum plot with disturbance.

### C. POINTING ACCURACY TEST

This test was performed to measure how precisely the servo can move a certain number of counts, and also determine how reproducible the movements are, in an absolute sense.

The setup of the test is shown in Figure 5.7. The test relies on the fact that for a small change in the reflected beam angle, the arc subtended by the beam at a distant target (piece of paper) is approximately a straight line. A solid state laser beam was shone on the mirror and it was intercepted at a distance of 20 m from the mirror on a piece of paper, so that the positions of the beam could be recorded. Table 5.1 summarizes the results and they are plotted in Figure 5.8. Because of inherent limitations in the length measurements, beam positions on the paper are uncertain to  $\pm 0.5$  mm.

Analysis of the data shows that the accuracy of the servo is well within the design target of one half encoder count.

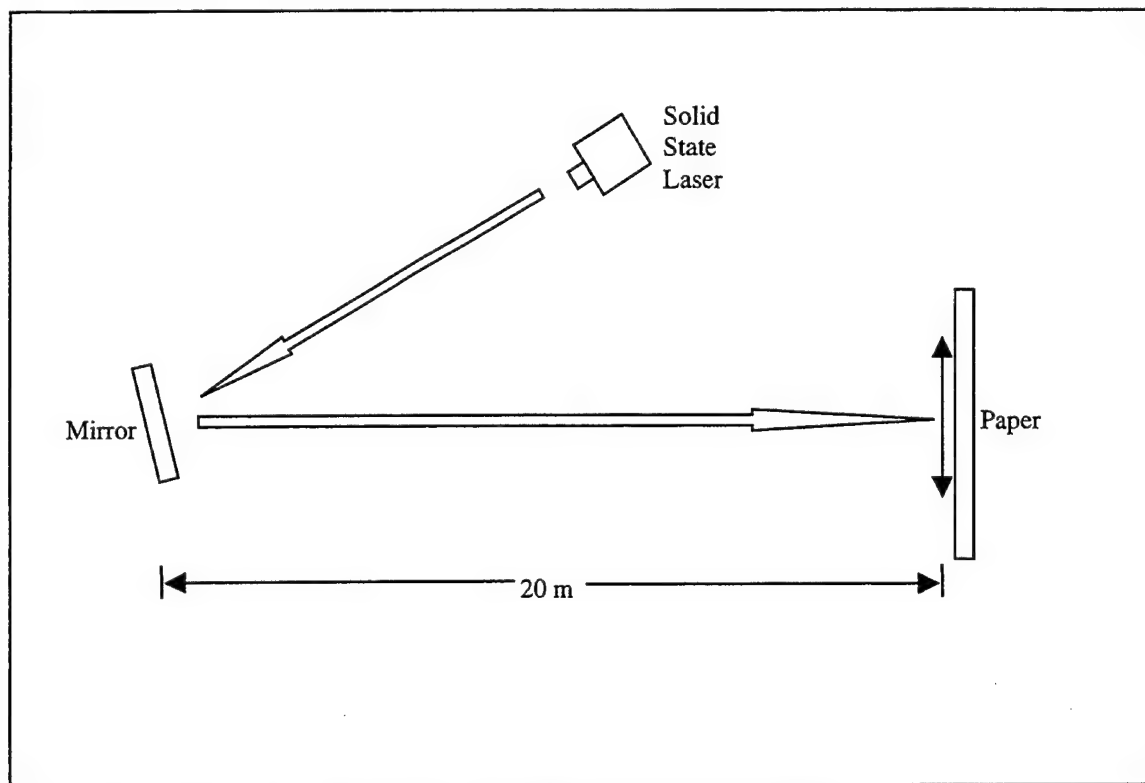


Figure 5.7. Pointing accuracy test setup.

Counts	Theoretical Distance [mm]	Measured Distance [mm]
0	0.0	0.0
1	1.7	2.0
4	7.0	7.0
15	26.2	27.0
30	52.4	51.0
50	87.3	88.0

Table 5.1. Accuracy test results.

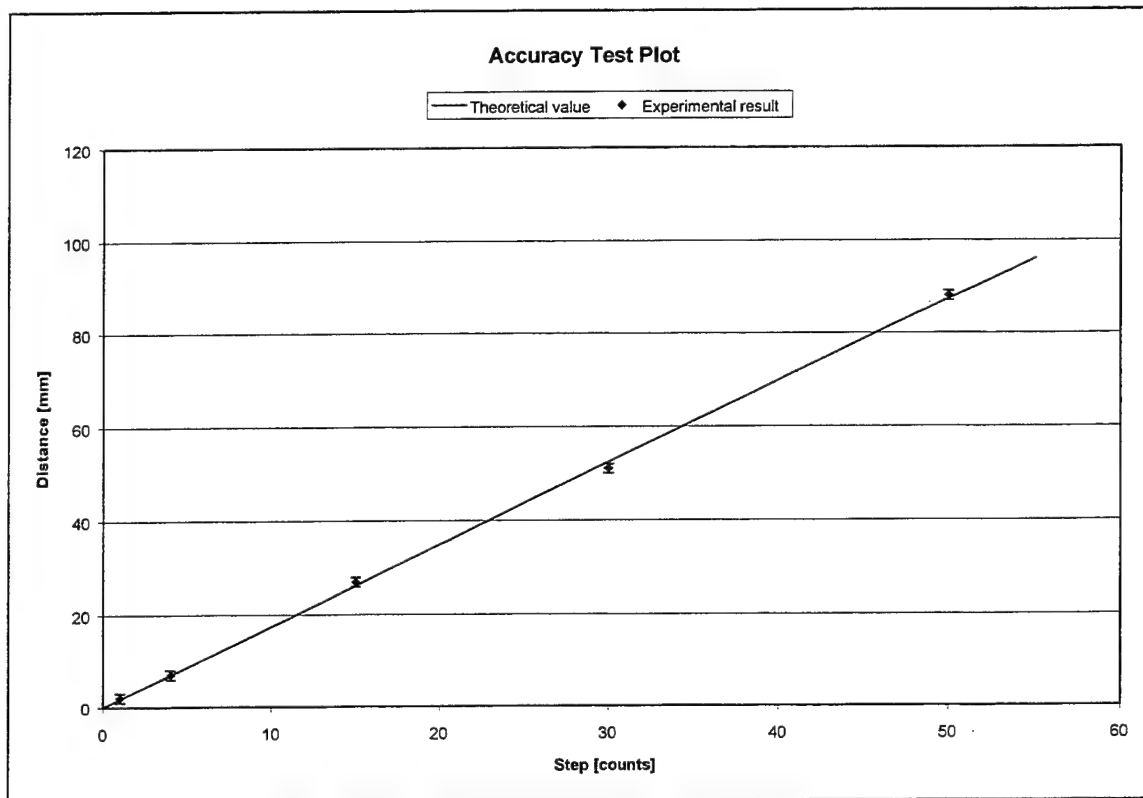


Figure 5.8. Plot of the accuracy test results.

To determine how well the servo can go back to the same position after several movements, it was made to repeatedly step 25 counts left and right of a known position. After 8 such iterations, the servo came back to the initial position within one half count, which is entirely consistent with the previous result.

#### D. IMAGING TEST ATTEMPTS

After the absolute pointing accuracy, precision, stability and repeatability were experimentally verified to have met the design criteria, initial attempts were made to use the scanning system in conjunction with the LINUS camera system and a USAF bar resolution chart to test the system's basic imaging capability. At the time of this writing,

we are experiencing difficulty with the camera system, and we have been unable to complete the camera-based tests. They have been deferred to a follow-up to this thesis research project.

THIS PAGE INTENTIONALLY LEFT BLANK

## VI. CONCLUSIONS

The design and development of LINUS is an ongoing project of the Department of Physics at the Naval Postgraduate School. The goal is to field-test the first version of the instrument by mid-2001.

The servo system of the instrument has been successfully integrated with the host computer with good relative performance. It is stable and has a final accuracy of  $\pm 1/2$  counts, equivalent to  $\pm 4.5$  arc-seconds. The final performance of the servo can only be assessed once the camera is integrated with the system and images are taken. The quality of the images will be the best performance measure for the system.

In case the quality of the images is not satisfactory due to the performance of the servo, the resolution of the encoder must be increased and re-tuning executed.

The follow-on work to this thesis should concentrate in the integration of the camera system with the host computer, and then the integration and synchronization of the camera with the servo system.



THIS PAGE INTENTIONALLY LEFT BLANK

## **APPENDIX A. HARDWARE DATA**

This Appendix shows the data sheets for the optomechanical scanner, encoder and DC motor. The optomechanical scanner was designed by Dr. Scott Davis. The data sheets of the encoder and scanner are those provided by the respective manufacturers.

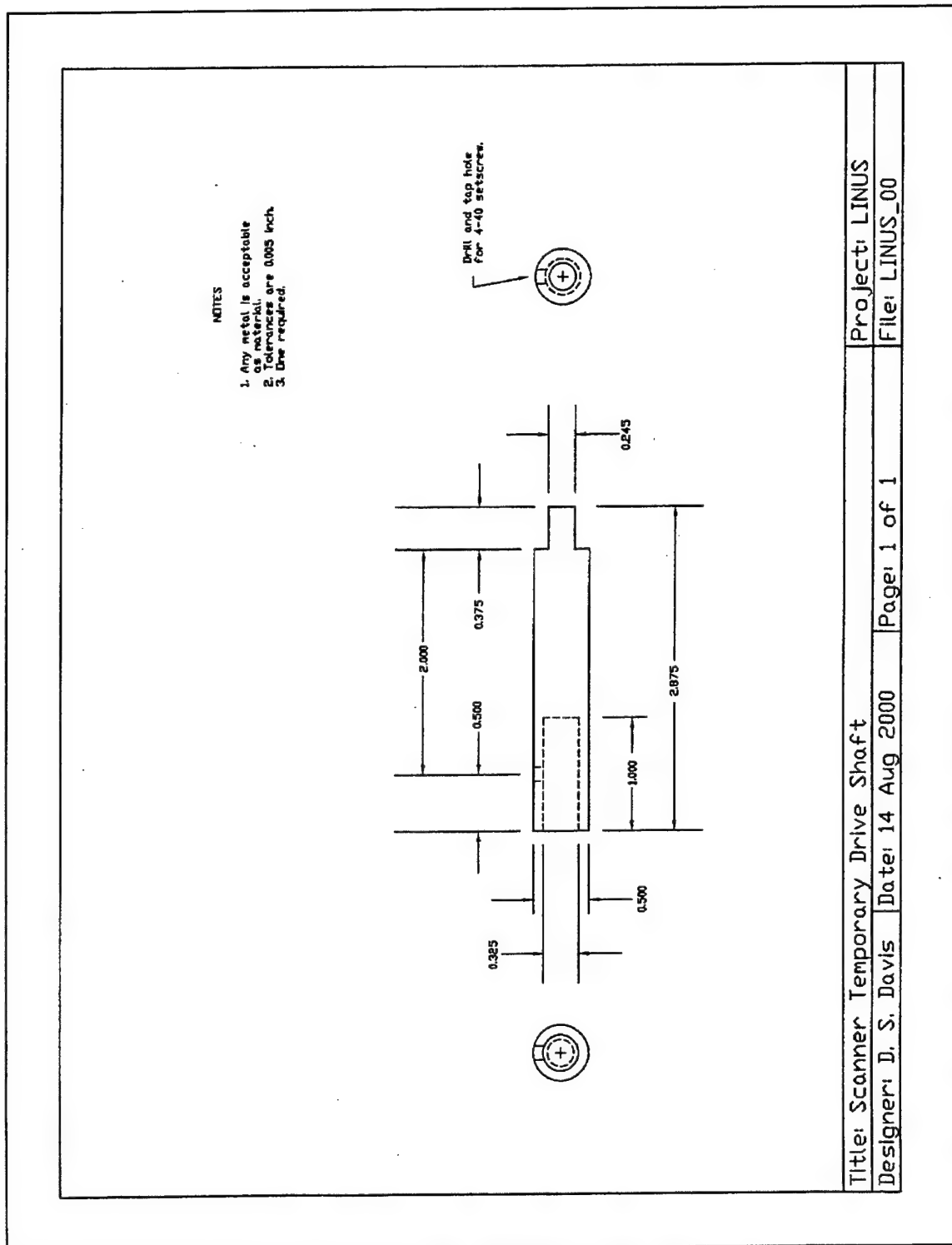


Figure A.1. Scanner temporary drive shaft.

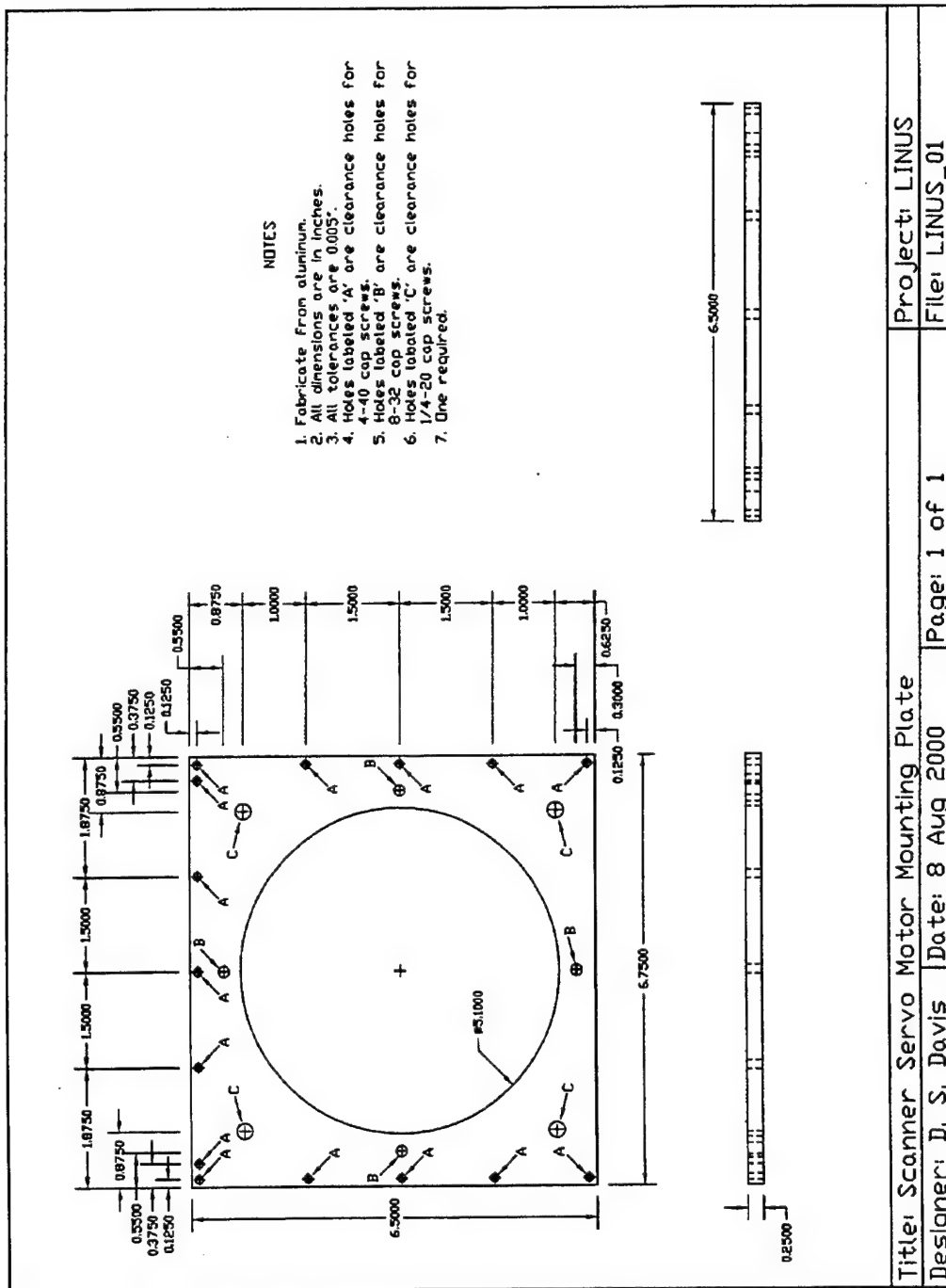


Figure A.2. Scanner servo motor mounting plate.

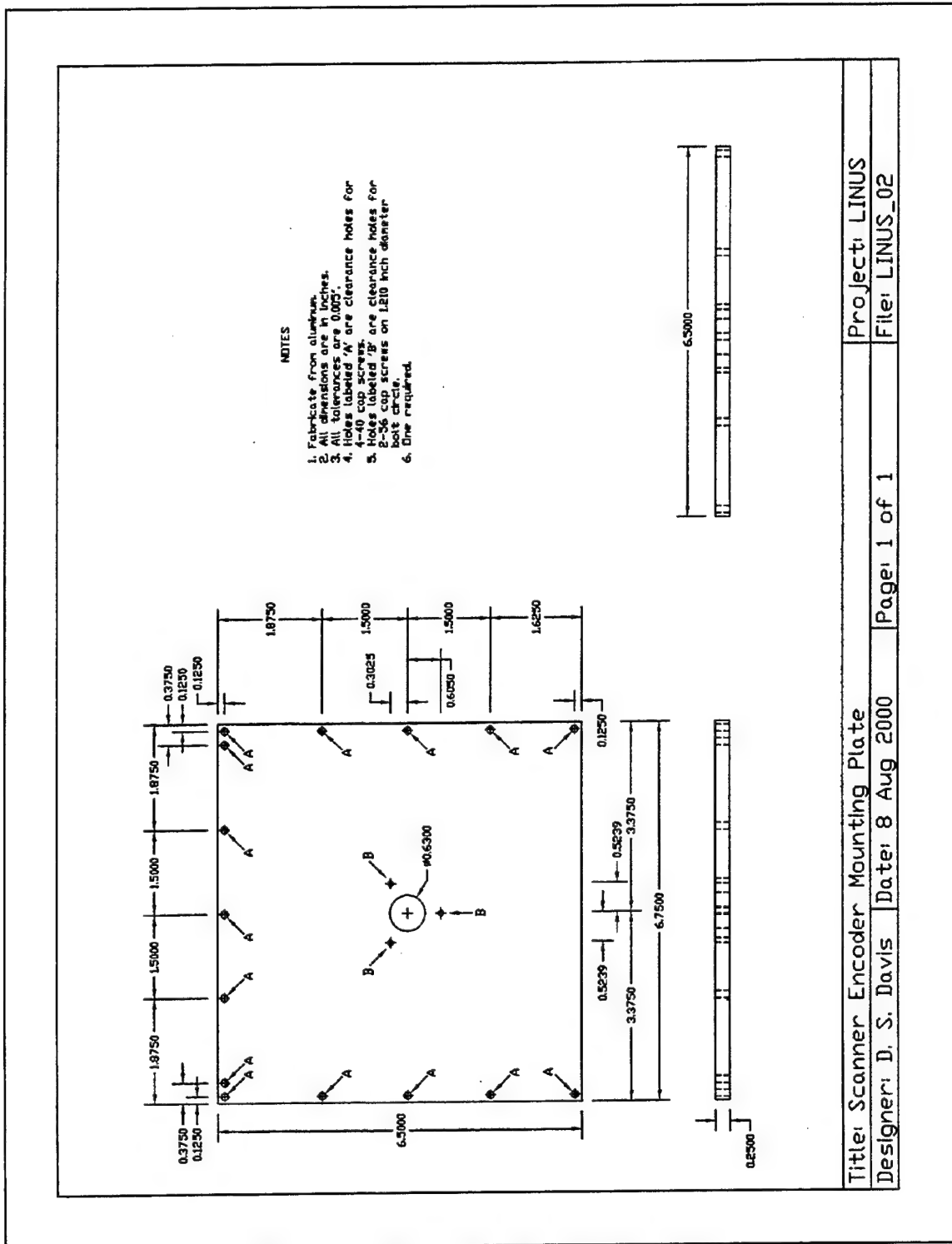
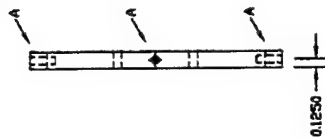
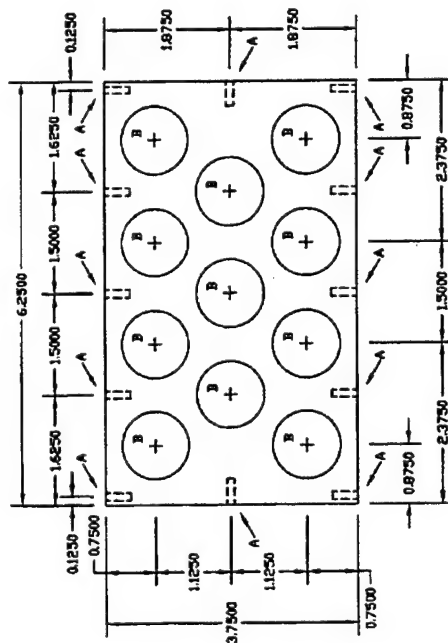
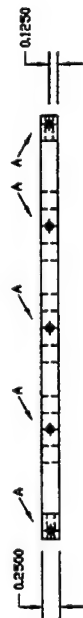


Figure A.3. Scanner encoder mounting plate.

- NOTES
1. Fabricate from aluminum.
  2. All dimensions are in inches.
  3. All tolerances are 0.005 inch.
  4. Holes labeled 'A' are to be tapped for 4-40 threads to a depth of 0.375 inch.
  5. Holes labeled 'B' are 1.000 inch in diameter.
  6. One required.



Title: Scanner Rear Panel	Project: LINUS
Designer: D. S. Davis	File: LINUS_03
Date: 10 Aug 2000	Page: 1 of 1

Figure A.4. Scanner rear panel.

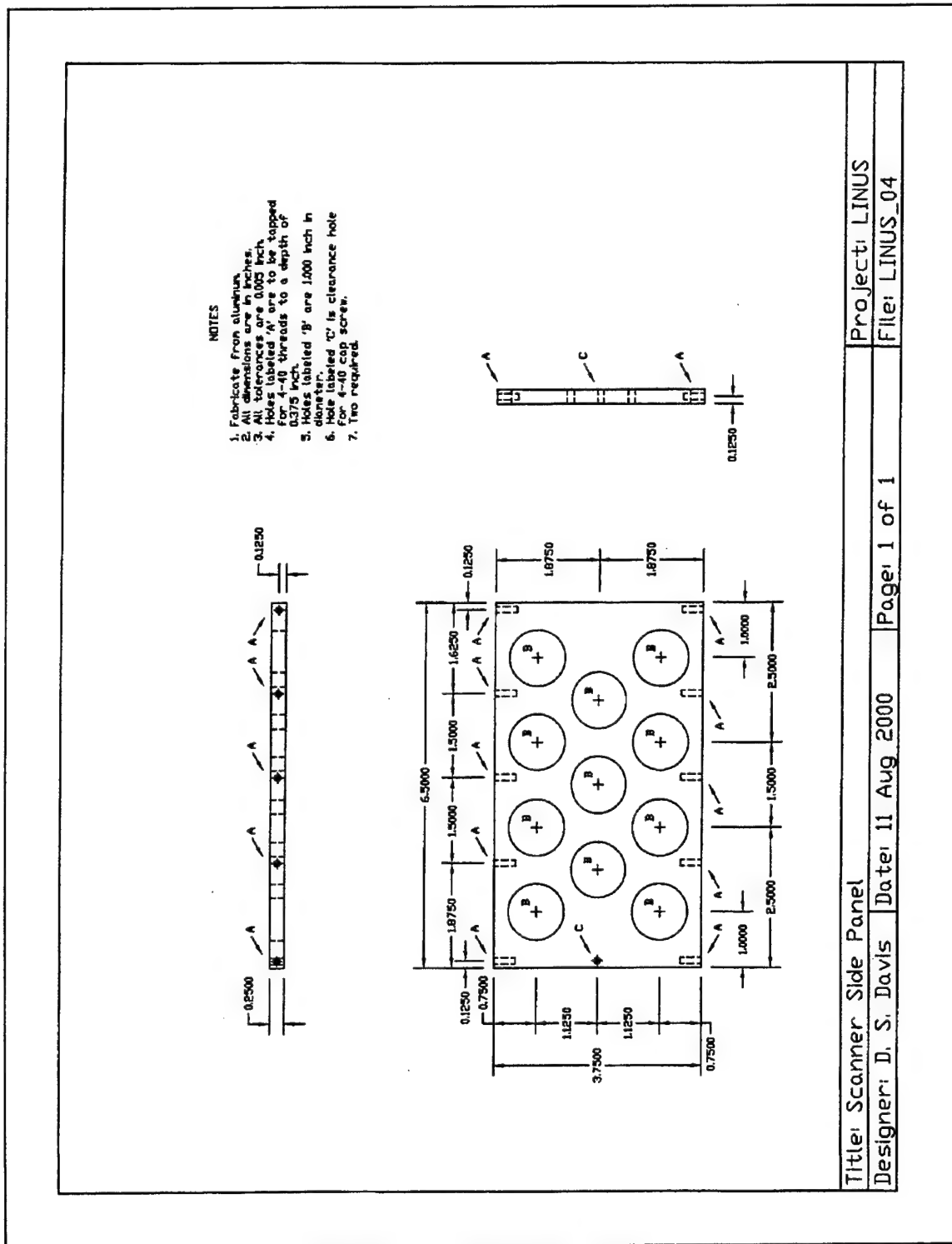


Figure A.5. Scanner side panel.

# NOTES

1. Fabricate from aluminum.
2. All dimensions are in inches.
3. Tolerance on diameter of coupling shaft hole (labeled 'C') diameter is 0.001 inch.
4. All other tolerances are 0.005 inch.
5. Holes labeled 'A' are to be tapped for 4-40 threads to a depth of 0.250 inch.
6. Holes labeled 'B' are for 8-32 setscrews and must be tapped along their entire length, into the coupling shaft hole.
6. Bore required.

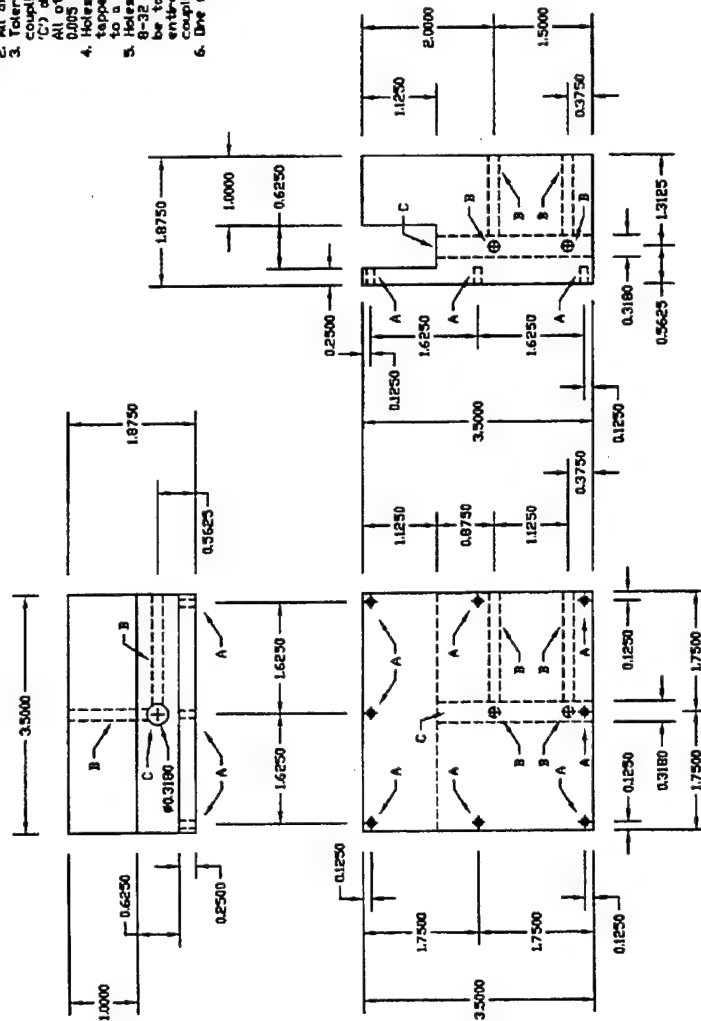


Figure A.6. Scanner Armature Substrate.

Title: Scanner Armature Substrate	Project: LINUS
Designer: D. S. Davis	File: LINUS_05
Date: 17 Aug 2000	Page: 1 of 1



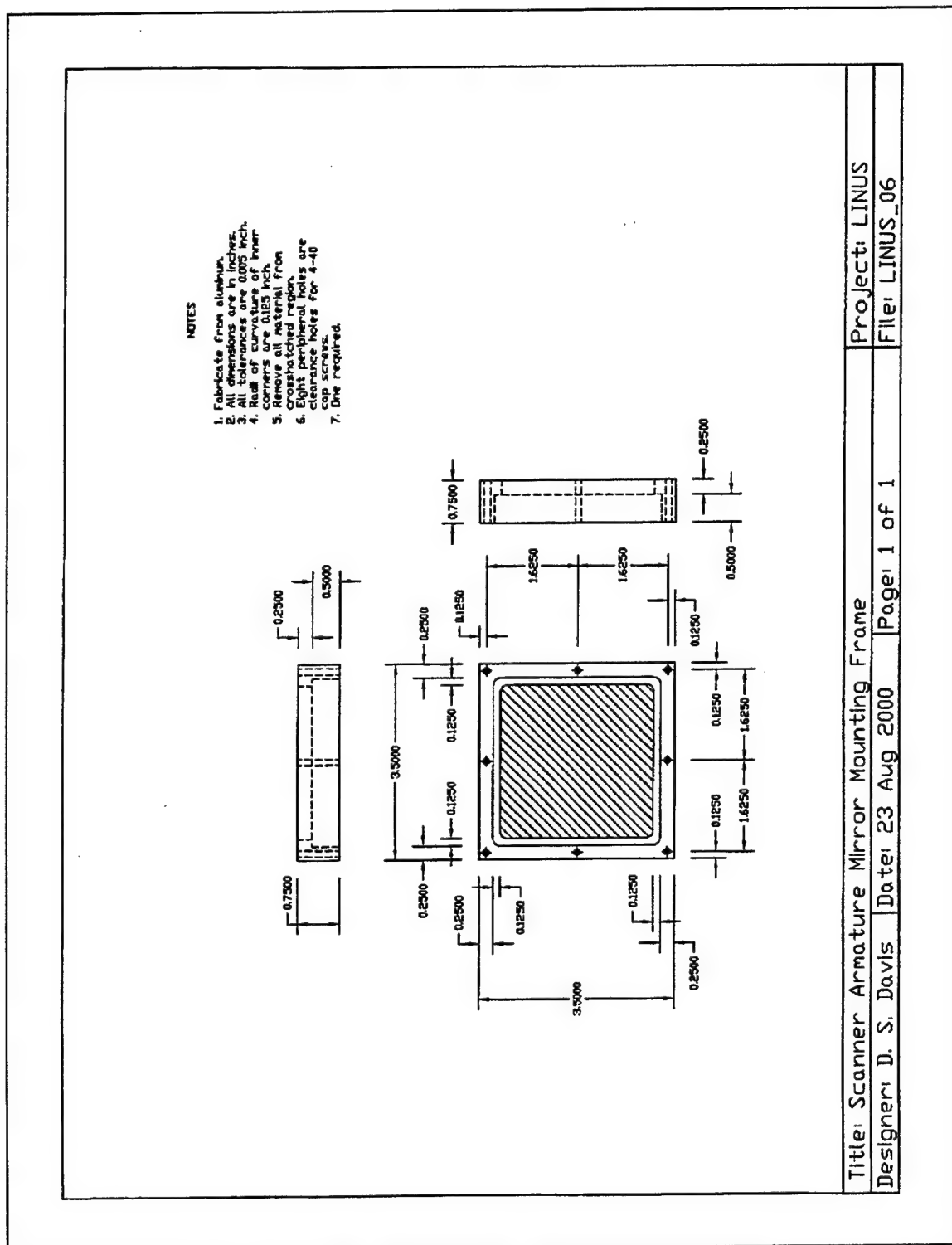
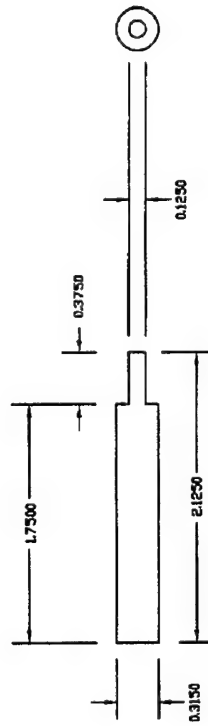


Figure A.7. Scanner armature mirror mounting frame.

NOTES

1. Fabricate from stainless steel.
2. All dimensions are 0.001 inch. Unstated tolerances are 0.005 inch.
3. One required.



Title: Scanner Armature Coupling Shaft	Project: LINUS
Designer: D. S. Davis	Page: 1 of 1
Date: 18 Aug 2000	File: LINUS_07

Figure A.8. Scanner armature coupling shaft.

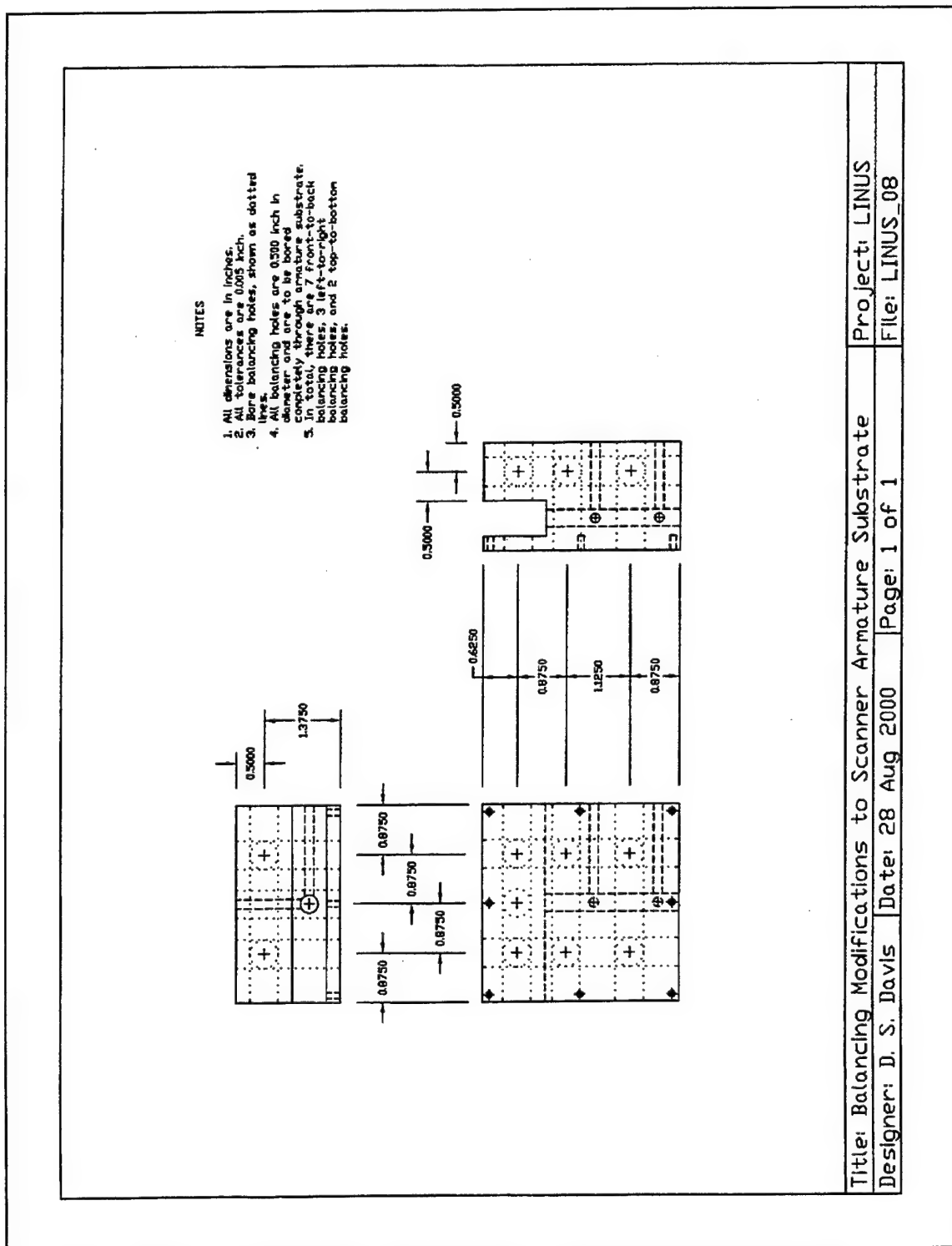


Figure A.9. Balancing modifications to scanner armature substrate.

## SPECIFICATIONS

	See Note	Model R135	Model R137
Maximum line count on disc		3600	
Maximum cycles/rev (quad sq waves)		36,000	
Max counts/rev (after quad decode)		144,000	
Internal square wave interpolation		1X, 2X, 5X or 10X	
Instrument error, $\pm$ arcsec	1, 2	70	
Quadrature error, $\pm$ electrical degrees	1, 3	24	
Interpolation error, $\pm$ quanta	1, 4	0.15	
Maximum output frequency, kHz			
1X square waves		100	
2X square waves		150	
5X square waves		300	
10X square waves		500	
Starting torque, in-oz (N-m) @20°C	6	S: 0.05 (3.5 x 10 <sup>-4</sup> )	B, C: 0.4 (2.8 x 10 <sup>-3</sup> )
Running torque, in-oz (N-m) @20°C	6	S: 0.015 (1.1 x 10 <sup>-4</sup> )	B, C: 0.1 (0.7 x 10 <sup>-3</sup> )
Moment of inertia, in-oz-s <sup>2</sup> (g-cm <sup>2</sup> )		4.5 x 10 <sup>-3</sup> (3.2)	
Maximum acceleration, rad/s <sup>2</sup>		3 x 10 <sup>6</sup>	
Operating temperature, °F (°C)		32 to 158 (0 to 70)	
Storage temperature, °F (°C)		0 to 160 (-18 to 71)	
Humidity, % rh, non-condensing		98	
Shock		50 g, 11 ms	
Vibration		15 g, 0-2000 Hz	
Maximum weight, oz (g)		2.1 (60)	2.7 (75)
Sealing		IP54	IP66, except IP64 at the shaft exit
Bearings		Grease-lubricated and sealed	
Maximum radial shaft load, lb (N)	5, 6	S: 2 (10)	

### NOTES:

1. **Total Optical Encoder Error** is the algebraic sum of *Instrument Error* + *Quadrature Error* + *Interpolation Error*. Typically, these error sources sum to a value less than the theoretical maximum. Error is defined at the signal transitions and therefore does not include quantization error, which is  $\pm 1/2$  quantum. ("Quantum" is the final resolution of the encoder, after user's 4X quadrature decode.) Accuracy is guaranteed at 20°C.
2. **Instrument Error** is the sum of disc pattern errors, disc eccentricity, bearing runout and other mechanical imperfections within the encoder. This error tends to vary slowly around a revolution.
3. **Quadrature Error** is the combined effect of phasing and duty cycle tolerances and other variables in the basic analog signals. This error applies to data taken at all four transitions within a cycle; if data are extracted from 1X square waves on a 1X basis (i.e., at only one transition per cycle), this error can be ignored.  
**Error in arcseconds = (3600) x (error in electrical degrees) ÷ (disc line count)**
4. **Interpolation Error** is present only when the resolution has been electronically increased to more than four data points per optical cycle. It is the sum of all the tolerances in the electronic interpolation circuitry.  
**Error in arcseconds = (1296000) x (error in quanta) ÷ (counts/rev)**
5. If higher load capacity is required, consult factory.
6. **S** = solid shaft version; **B** = blind hollow shaft with external tether; **C** = blind hollow shaft with internal coupling.

As part of our continuing improvement program, these specifications are subject to change without notice.

GURLEY PRECISION INSTRUMENTS - TROY, NY - 800.759.1844 FAX 518.274.0336 - WWW.GURLEY.COM - ENCODERS@GURLEY.COM

Figure A.10. Encoder specifications.

## ELECTRONICS OPTIONS

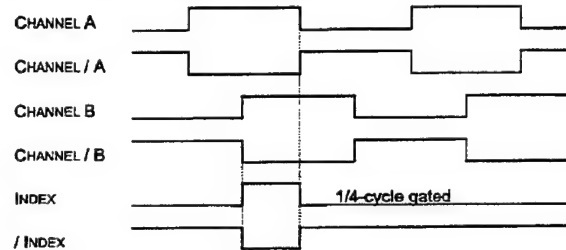
### INPUT POWER

+5 VDC @100 mA max.

### SQUARE WAVE OUTPUT – OUTPUT CODE L

Quadrature square waves at 1, 2, 5 or 10 times the line count on the disc. On all channels: EIA/RS-422 balanced differential line driver, protected to survive an extended-duration short circuit across its output. May be used single-ended for TTL-compatible inputs. Index is ¼-cycle wide, gated with the high states of channels A and B.

#### OUTPUT WAVEFORMS (CW rotation shown)



### BUFFERED SINUSOID OUTPUT – OUTPUT CODE B

The output device is an op-amp referenced to  $(50\% \pm 3\%) \times V_{CC}$ . Typical signal roll-off at 100 kHz  $\leq 3$  dB. Signal values at 1 kHz with 4.7 k $\Omega$  load to common (20°C):

Peak-to-peak signal amplitudes, SIN and COS:	$1.0 \pm 0.1$ V
Amplitude ratio, min chan to max chan:	0.9 to 1.0
Peak-to-peak signal amplitude, index channel:	$\geq 0.75$ V

### BUFFERED SINUSOID OUTPUT – OUTPUT CODE M

Same as OUTPUT CODE B, except SIN, COS and IND complements are also provided.

### EXTENDED RESOLUTION

The R135 and R137 offer resolution up to 36,000 cycles/rev (up to 144,000 counts/rev after user's 4X quadrature decode) with internal electronics. If finer resolution is required (up to 288,000 counts/rev), the HR2A external electronics package can be used with either encoder. The HR2A can also provide interpolation factors other than 2, 5 or 10, which are available internally in the R135 and R137. The encoder must be ordered with output code B and connector code Q. (See separate HR2A data sheet for details).

GURLEY PRECISION INSTRUMENTS - TROY, NY - 800.759.1844 FAX 518.274.0336 - WWW.GURLEY.COM - ENCODERS@GURLEY.COM

Figure A.11. Encoder specifications.

## SPECIFICATIONS

### ELECTRICAL CONNECTIONS

	CONN. CODE	P	Q	R	S
	CONN. TYPE:	NONE	DA-15P	DE-15P	DE-9P
	FUNCTION:	COLOR	PIN #	PIN #	PIN #
Square Wave Output (output code L)	A	Yellow	8	8	4
	/A	Brown	7	7	8
	B	Green	5	5	3
	/B	Orange	4	4	7
	IND	Blue	2	2	2
	/IND	White	1	1	6
	+V	Red	10	10	5
	COMM	Black	13	13	9
Buffered Sinusoid Output (output code B)	CASE	See Note 1	9	9	1
	SIN	Yellow	9		
	COS	Green	11		
	IND	Blue	5		
	+V	Red	4		
	COMM	Black	15		
	CASE	See Note 1	8		
	MATING CONN.	-	M01	M05	M06

NOTE:

1. Model R135: The gray wire is connected to the encoder case.

Model R137: The bare wire (shield) is connected to the encoder case.

2. Channel A leads Channel B for clockwise shaft rotation, viewed from the shaft end.

### FLEXIBLE SHAFT COUPLINGS

	External Tether Mount (for B version)	Internal Shaft Coupling (for C version)	SCA-Shaft Coupling (for S version)
Wind-up, arcs/in-oz (arcs/Nm)	Negligible	Negligible	9.7 (1375)
Max. parallel offset, in (mm)	0.003 (0.08)	0.004 (0.1)	0.020 (0.50)
Max. angular misalignment, degrees	2	0.5	1
Max. axial extension or compression, in (mm)	0.005 (0.13)	None	0.020 (0.50)
Moment of inertia, in-oz-s (g-cm <sup>2</sup> )	N/A	N/A	4.3 x 10 <sup>-4</sup> (30)
Weight, oz (g)	Negligible	N/A	1.0 (30)

NOTE: Flexible couplings are intended to absorb normal installation misalignments and run-outs in order to prevent undue loading of the encoder bearings. To realize all the accuracy inherent in the encoder, the user should minimize misalignments as much as possible.

Model number of the shaft coupling for S version (use BASE CODE C or E with 1/4" shaft dia.) is SCA-04E-XXX, where XXX = user's shaft diameter. Select XXX from the following table:

04E	1/4"
05E	5/16"
06E	3/8"
04M	4 mm
06M	6 mm
10M	10 mm

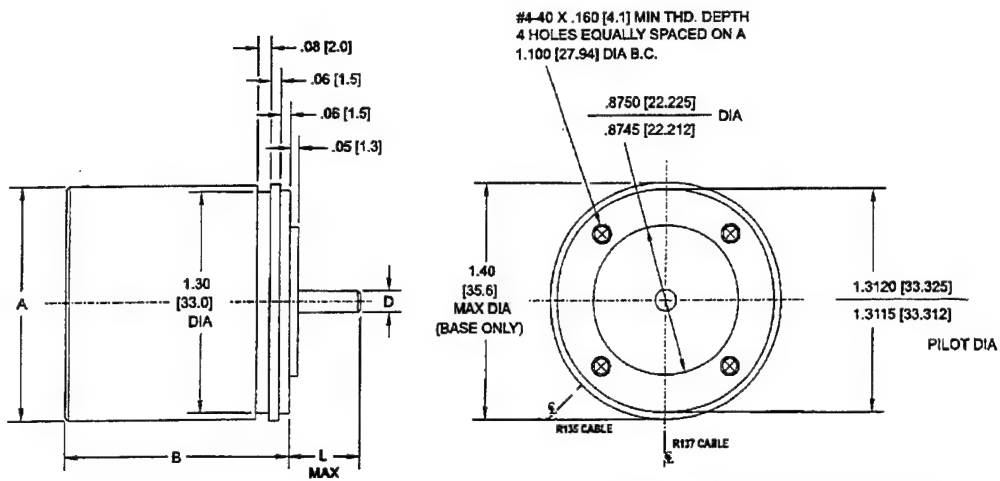
### AVAILABILITY OF DIFFERENT SHAFT DIAMETERS (blank = not available)

BASE CODE:	A	B	C	D	E	F	G
R135	4 mm		1/8", 1/4"	1/8"		3 mm	3 mm
R137		4 mm	1/8", 1/4"	1/8"	1/4"	3 mm	3 mm

GURLEY PRECISION INSTRUMENTS - TROY, NY - 800.759.1844 FAX 518.274.0336 - WWW.GURLEY.COM - ENCODERS@GURLEY.COM

Figure A.12. Encoder specifications.

## DIMENSIONS

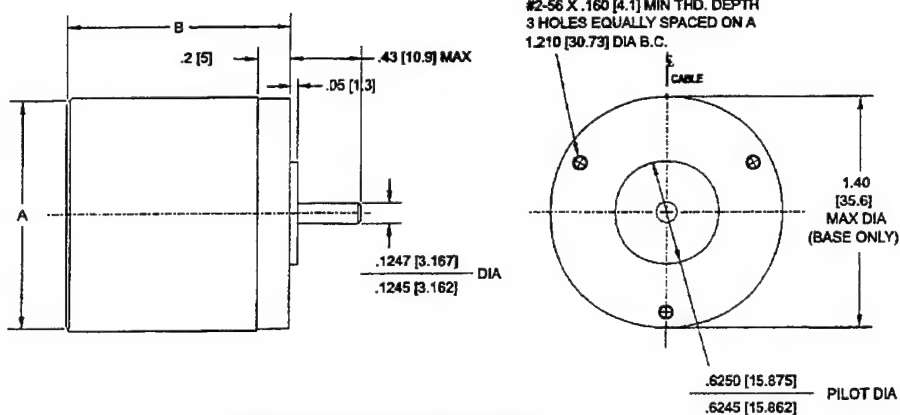


MODEL R13xS WITH BASE CODE C

FOR BASE  
CODES C & D

	R135	R137
A COVER DIA	1.38 [35.0]	1.44 [36.5]
B LENGTH	1.36 [34.5] MAX	1.46 [37.0] MAX

DIA CODE	D	L
02E	.1247/.1245 [3.167/3.162]	.43 [10.9]
04E	.2447/.2445 [6.342/6.337]	.63 [16.0]



MODEL R13xS WITH BASE CODE D

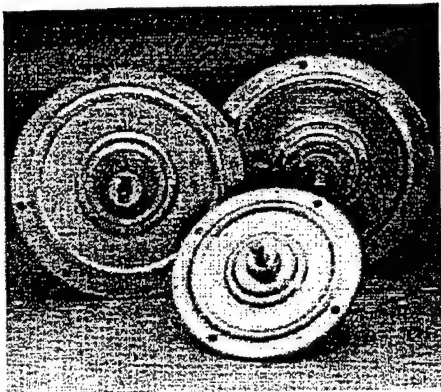
ALL DIMENSIONS IN INCHES [MM]

GURLEY PRECISION INSTRUMENTS - TROY, NY - 800.759.1844 FAX 518.274.0336 - WWW.GURLEY.COM - ENCODERS@GURLEY.COM

Figure A.13. Encoder specifications.

## Ferrite Series ServoDisc

### INTRODUCTION



- Options:
  - Tachometers
  - Encoders
  - Fail-safe brakes

#### Compatible Products

- KXA Plus Amplifier
- EM19 Linear Amplifier

- 16 to 56 oz-in (11-40 N-cm) Continuous Torque
- 4.0 to 5.1" OD Round Frame
- Ultrathin Pancake Motor

Ferrite Series ServoDisc motors employ the unique Kollmorgen flat disc armature and ultraflat package to create a low cost ServoDisc motor.

- Extremely good speed control with zero cogging and low RFI
- Very long brush life
- Flat ServoDisc motors are ideal for many applications:
  - Save space and weight in applications requiring a low profile motor
  - Large torsional stiffness for precision control of speed and acceleration
- Low inertia, DC servomotor
- Low axial profile
- High-pulse torque capability
- No cogging even at low operating speeds

Figure A.14. Motor specifications.



# Ferrite Series ServoDisc

## PERFORMANCE DATA

Performance Specifications	Symbol	Units	9P/9FS	9FST	12FLR/12FLRB/ 12FLRS	12F/12FB/ (12FS)	12FV/12FVB/ 12FVS
Peak Torque	$T_p$	oz-in	198	189	393	478	549
		N-cm	140	133	278	338	388
Rated Speed	N	RPM	3000	3000	3000	3000	3000
Rated Continuous Torque @ 25°C	$T_{25}$	oz-in	17	15	31	40	44
		N-cm	12	11	22	28	31
Rated Continuous Torque @ 40°C	$T_{40}$	oz-in	15	13	29	36	39
		N-cm	10.6	9	20	26	27
Rated Power Output	P	Watts	37	33	68	88	96
Maximum Recommended Speed	N <sub>max</sub>	RPM	6000	6000	6000	6000	6000
Continuous Stall Torque	$T_s$	oz-in	16	15	31	41	46
		N-cm	11	11	22	29	32
Cogging Torque	$T_c$	oz-in	0	0	0	0	0
<b>Electrical Specifications</b>							
Rated Terminal Voltage	E	Volts	14.6	14.4	11.7	21.6	16.5
Rated Continuous Current	I	Amps	6.8	6.60	12.10	7.5	10.3
Peak Current	$I_p$	Amps	70	70	136	81	116
Continuous Stall Current	L	Amps	6.3	6.2	11.9	7.4	10.3
<b>Winding Specifications</b>							
Terminal Resistance ± 10%	$R_1$	Ohms	0.950	0.950	0.400	0.860	0.48
Armature Resistance ± 10%	$R_2$	Ohms	0.640	0.640	0.210	0.610	0.29
Back EMF Constant ± 10%	$K_e$	V/KRPM	2.39	2.30	2.45	5.00	4.00
Torque Constant ± 10%	$K_t$	oz-in/Amp	3.23	3.11	3.32	6.77	5.41
		N-cm/Amp	2.28	2.20	2.34	4.78	3.82
Viscous Damping Constant	$K_d$	oz-in/KRPM	0.3	0.3	0.6	0.7	1.0
		N-cm/KRPM	0.2	0.2	0.4	0.5	0.7
Armature Inductance	L	μH	<0.03	<0.10	<0.03	<0.05	<0.03
Temperature Coefficient of $K_e$	C	%/°C Rise	-0.19	-0.19	-0.19	-0.19	-0.19
Number of Commutator Bars	Z		117	117	141	141	105
<b>Mechanical Specifications</b>							
Moment of Inertia	$J_m$	oz-in-sec <sup>2</sup>	0.0052	0.0080	0.0190	0.0190	0.0220
		kg-cm <sup>2</sup>	0.37	0.56	1.34	1.34	1.62
Average Friction Torque	$T_f$	oz-in	2.5	2.5	3.5	3.0	3.5
		N-cm	1.8	1.8	2.5	2.1	2.5
Weight	W	lbs	1.2	1.2	2.2	2.2	2.2
		kg	0.5	0.5	1.0	1.0	1.0
Diameter	D	in	4.72	4.72	5.98	5.98	5.98
		mm	119.9	119.9	151.9	151.9	151.9
Length	LG	in	0.75	1.36	0.80	0.80	0.80
		mm	19.1	34.5	20.3	20.3	20.3
<b>Figure of Merit</b>							
Peak Acceleration	$A_p$	kRad/sec <sup>2</sup>	38.1	23.6	21.0	25.1	25.0
Mechanical Time Constant	$T_m$	ms	44.00	72.80	50.70	35.40	30.4
Electrical Time Constant	$T_e$	ms	<0.05	<0.16	<0.12	<0.07	0.34
Continuous Power Rate	$P_c$	kW/sec	0.3	0.2	0.3	0.6	0.6
<b>Thermal Specifications</b>							
Thermal Resistance at Rated Speed	RAAR	°C/Watt	2.00	2.00	1.70	1.70	1.70
Thermal Resistance at Stall	RAAS	°C/Watt	2.52	2.52	2.03	2.03	2.03
<b>Tachometer Specifications</b>							
Output Voltage	V	Volts/KRPM	—	1.10	—	—	—
Maximum Ripple Peak to Peak	$V_m$	%	—	5.0	—	—	—
Linearity of Output Voltage	LIN	%	—	0.14	—	—	—

### Notes:

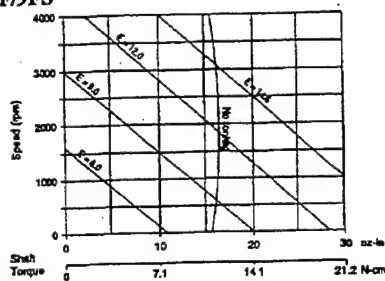
- All values are based upon a 150°C armature temperature limit and with the motor mounted on an 8" x 16" x 3/8" aluminum heatsink with no forced air cooling. Other voltages, speeds, and torques are achievable as long as the max armature temperature of 150°C is not exceeded.
- Max air flow (lb/min) = air volume (CFM) x air density (lb/ft<sup>3</sup>).
- Terminal resistance is measured at 4.0 amps.  $R_T$  varies as a function of applied current.
- Unless otherwise noted, all specifications above apply at 25°C.
- Peak torque and current is calculated based on max pulse duration of 50 milliseconds and a 1% duty cycle.
- The operating current can be calculated as:  $I = (\text{Shaft torque} + T_f + ED \times N/1000) / K_T$
- The operating voltage can be calculated as:  $V = K_e \times (N/1000) + R_T \times I$
- Tachometer ripple measured with a resistive load of 1 kohm and a single low pass filter with 3db cut off at 500 Hz.
- Tachometer minimum measured with a resistance of 370 ohms.
- Bidirectional tolerance of tachometer will not exceed 3%.

Figure A.15. Motor specifications.

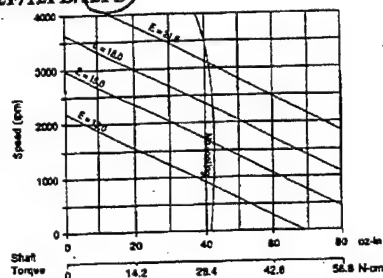
# Ferrite Series

## PERFORMANCE DATA

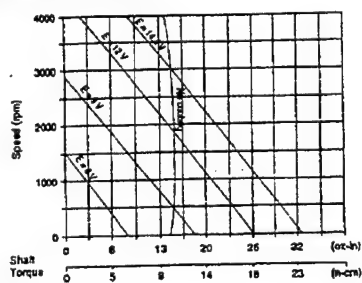
9F/9FS



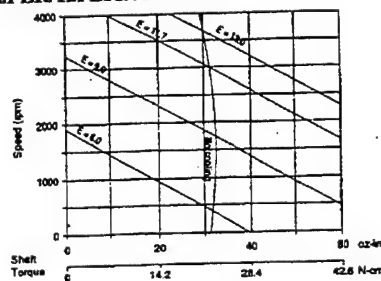
12F/12FB/12FS



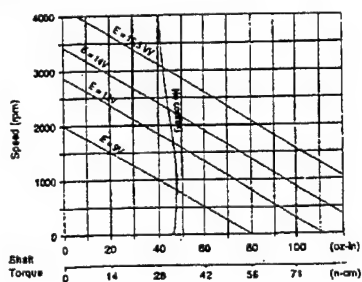
9FST/9FGT/9FGHDT



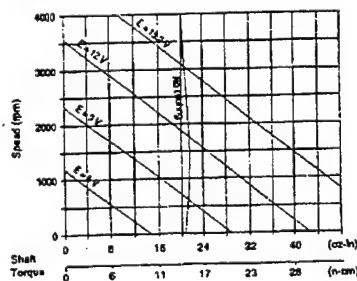
12FLR/12FLRB/12FLRS



12FV/12FVB/12FVS



9FHB-44



### Notes:

- All curves are drawn for a fixed armature temperature of 150°C.
- The motor can be operated at any point on the graph below 4000 RPM. Higher speeds are possible for some applications. Contact a Kollmorgen Sales Office for more details.
- Determine voltage required for a desired combination of speed and torque by estimating it as a line parallel to one of the constant terminal voltage (E) lines.

### D. The operating current can be calculated as:

$$I = (\text{Shaft torque} + TF + KD \times N/1000)/KT$$

### E. The operating voltage can be calculated as:

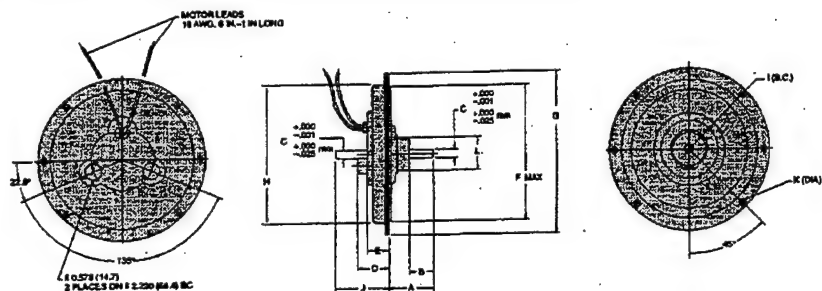
$$V = KE \times N/1000 + RT \times I$$

Figure A.16. Motor specifications.

## Ferrite Series ServoDisc

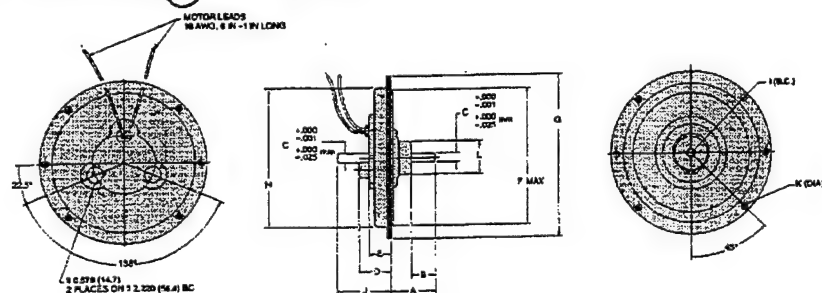
## DIMENSIONS

**Motor Types: 9F, 12F, 12 FLR, 12FV AND 12FB, 12FLRB, 12FVB**



Motor Types	Units	A	B	C	D	E	F	G	H	I	J (optional)	K	L
9F	in	1.19	0.593	.3125	1.03	0.75	4.0	4.72	3.91	4.33	1.98	0.22	0.81
	mm	30.16	15.06	7.94	26.16	19.05	101.6	120.0	99.2	110.0	50.3	5.6	20.64
12F, 12FLR, 12VF, 12FLRB, 12VFB	in	1.69	0.92	0.315	1.17	0.80	5.08	5.98	5.11	5.59	2.12	0.22	1.22
	mm	42.9	23.4	8.00	29.8	20.2	129.0	151.9	129.8	142.0	53.8	5.6	31.0

**Motor Types: 9FS, 12FS, 12FLRS, 12FVS**



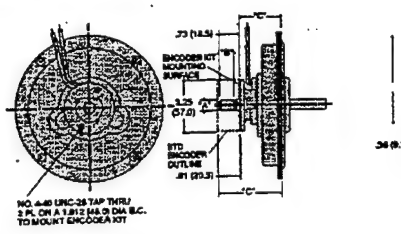
Motor Types	Units	A	B	C	D	E	F	G	H	I	J (optional)	K	L
9FS	in.	1.0	0.75	0.250	1.03	0.75	4.0	4.72	3.91	4.33	1.98	0.22	.31
	mm	25.4	19.05	6.35	26.16	19.05	101.6	119.9	99.2	110.0	50.3	5.6	7.9
12FS, 12FLRS, 12FVS	in.	1.0	0.75	0.315	1.39	0.80	5.06	5.98	5.11	5.59	2.12	0.22	
	mm	25.4	19.05	8.0	35.31	20.24	129.03	151.89	129.8	142.0	53.8	5.6	

Figure A.17. Motor specifications.

## Ferrite Series ServoDisc

## DIMENSIONS

### Motor with Encoder and Motor Prepared for Encoder



Motor Types	Units	A	B	C	D
9FS	in	0.2497 + 0.0000/-0.0005	0.67	1.26	2.07
	mm	6.342 + 0.000/-0.013	17.0	32.0	52.5
12FS, 12FLRS,	in	0.3147 + 0.0000/-0.0005	0.65	1.38	2.20
12FVS	mm	7.994 + 0.000/-0.013	16.5	35.0	56.0

Note: Other Windings/Voltages available.

Motor Types	Radial Load		Axial Load		End Play Under Axial Load		Run Out in per in of Shaft Length
	lbs	kg	lbs	kg	in	mm	
9F	2.5	1.13	2.5	1.13	0.003	0.076	0.002
9FS	3	1.36	3	1.36	0.001	0.025	0.001
12F, 12FLR, 12FV	2.5	1.13	2.5	1.13	0.003	0.076	0.002
12FB, 12FLRB, 12FVB	7	3.18	10	4.54	0.001	0.025	0.001
12FS, 12FLRS, 12FVS	7	3.18	10	4.54	0.001	0.025	0.001

MOTOR SELECTION FOR FERRITE SERIES				
Motor Types	Motor Alone	Motor with Rear Shaft	Motor Prep. for Encoder	Motor with Integral Optical Encoder Type M2 (500 lines Max)
9F, 12F, 12FLR, 12FV	Lowest cost	YES (option)	NO	NO
12FB, 12FLRB, 12FVB	Front spindle Ball bearings	YES (option)	NO	NO
9FS, 12FS, 12FLRS, 12FVS	Rear spindle Ball bearings	YES (option)	YES (option)	YES (option)

### FERRITE MOTOR WITH INTEGRAL TACHOMETER

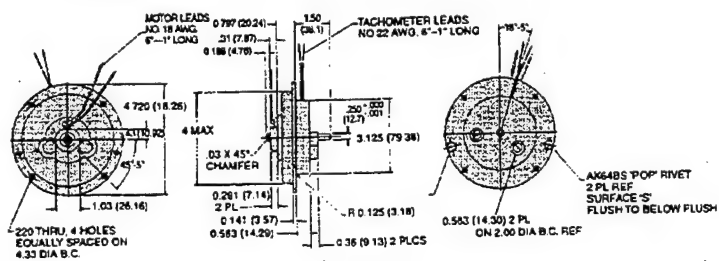


Figure A.18. Motor specifications.

THIS PAGE INTENTIONALLY LEFT BLANK

## **APPENDIX B. LABVIEW PROGRAMS**

This Appendix lists and explains the LabView code implemented to drive the servo system in the laboratory. It is intended to aid those who follow in the development of LINUS, and not as a LabView tutorial. The explanation assumes that the reader is familiar with the programming language G, LabView and the Flexmotion VI library.

The programs are stored in the path:

`C:\Program Files\National Instruments\LabVIEW\Linus\`

Since programs are executed from left to right, individual VI's will be explained in that order.

### **1. LINUS INITIALIZATION.VI**

Figures B.1 and B.2 show the program "Linus Initialization.vi," whose purpose is to initialize the Flexmotion board to the required parameters for operation. Numbers, that are not in the original code, have been added to the Figures to identify the different components of the program and ease the explanation. The action performed by each VI depends on the actual input parameters.

#### **1. Board Id**

Board Id is a constant set to the value 1 that identifies the Flexmotion board.

## 2. Clear Power Up Status

The Clear Power Up Status VI sets the board to a known state by forcing the initialization and trajectory parameters to their default values. Default values can be found in the Flexmotion VI Library Help.

## 3. Stop Motion

Orders a Kill Stop to the six motion axes of the board. Ensures that power to the motor is off during the rest of the setup procedure.

## 4. Enable Axes

Disables the six axes in order to change some of the default values.

## 5. Configure Axis Resources

Configures axis 1 which is the one chosen to drive the electric motor, to work with the Encoder 1 input and DAC 1 output resources.

## 6. Enable Axes

Enables axis 1.

## 7. Load All PID Parameters

Sets the PID parameters to the following values:  $K_P=300$ ,  $K_I=5$ ,  $I_L=1000$ ,  $K_D=4000$ ,  $T_D=3$ , and the rest are left at 0.

## 8. Load Counts/Steps per Revolution

Sets the quadrature counts per revolution to 144,000.

9. Configure Inhibit Outputs

Disables the per-axis inhibit outputs.

10. Set Limit Input Polarity

Sets both the forward and reverse limit inputs to inverting logic (active-low).

11. Set Home Input Polarity

Sets the polarity of the home input to inverting logic.

12. Enable Limits

Disables forward and reverse limit inputs.

13. Enable Home Inputs

Disables the home input.

14. Set Operation Mode

Sets the operation mode for axis 1 to Relative Position.

15. Load Following error.

Sets the following error trip point to 32767 counts.

16. Load Velocity in RPM

Sets the maximum trajectory velocity to 10 RPM.

17. Load Accel/Decel in RPS/sec

Sets both the acceleration and deceleration to a maximum of 20 RPS/sec.



#### 18. Stop Motion

Executes a Halt Stop to axis 1.

#### 19. Load Velocity Override

Sets the velocity scaling to 100%.

#### 20. Configure Move Complete Criteria

Sets the move complete criteria to the following: motor must be stopped and with 0 error position.

#### 21. Configure Velocity Filter

Sets the time constant for the velocity filter to 10 sample periods, and sets the velocity threshold to 1 count/sample period.

#### 22. Bd Id Out

Bd Id Out is an indicator that indicates completion of the program by displaying the number of the axis in the front panel.

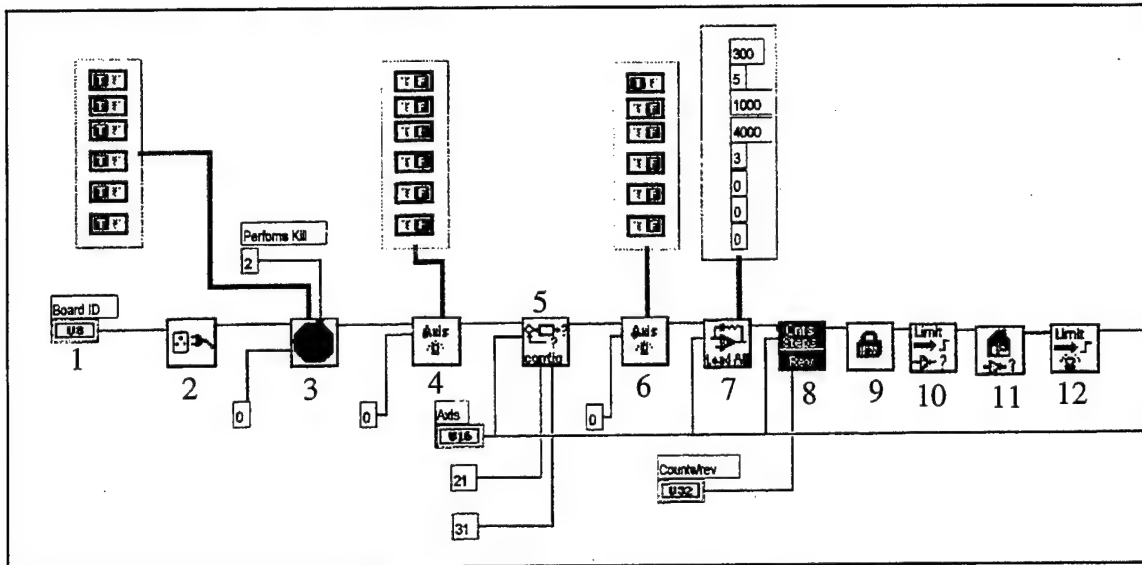


Figure B.1. Linus Initialization.vi.

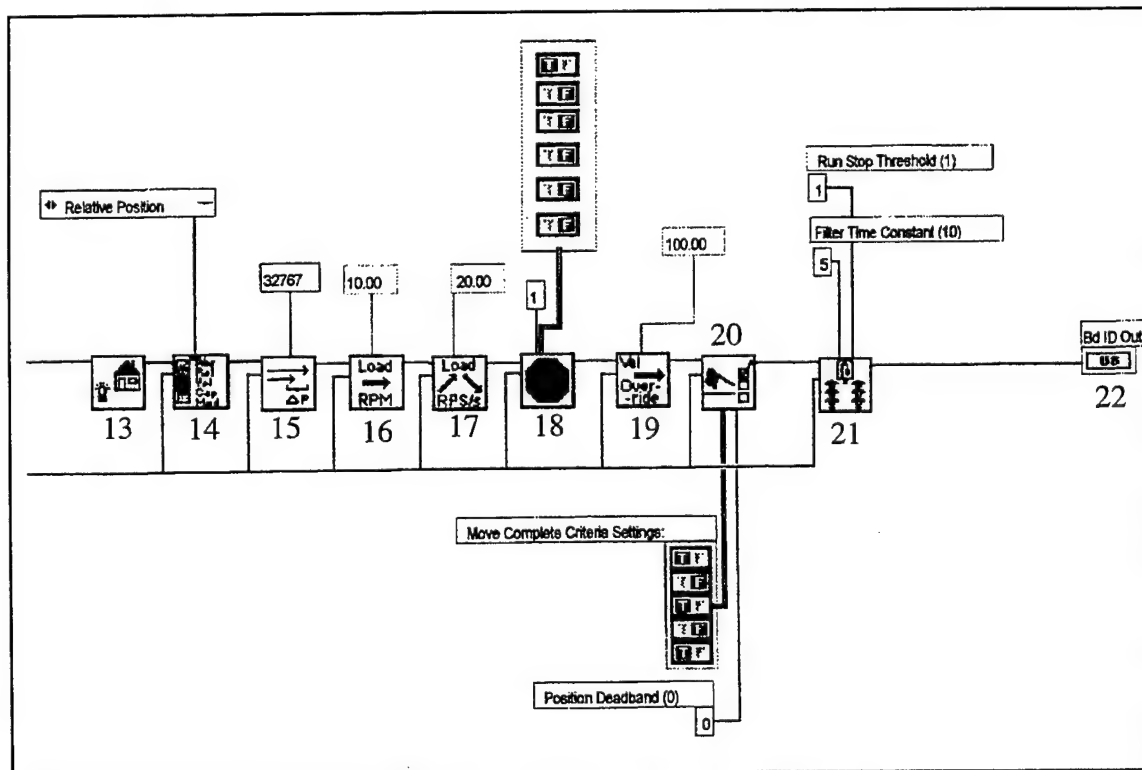


Figure B.2. Linus Initialization.vi (continued).

## 2. LINUS STEPPING PROGRAM.VI

“Linus Stepping Program.vi” allows the operator to make the servo move a number of steps, of a certain amplitude (number of counts), and in either the clockwise (CW) or counterclockwise (CCW) direction (looking at the motor from above). The inputs that the operator must provide are two: the number of steps, and the number of counts each step must be. A positive number of counts gives way to CCW motion, while a negative number generates CW motion. The program is shown in Figures B.3 and B.4.

### 1. Board Id

Board Id is a constant set to the value 1 that identifies the Flexmotion board.

### 2. Begin Program Storage

Begins storing program 1 onboard Flexmotion.

### 3. Load Constant to Variable

Loads the number of steps input by the operator into variable 1.

### 4. Load Constant to Variable

Loads the initial value 0 of the step counter into variable 2.

### 5. Load Constant to Variable

Loads the size of the increment (1) into variable 3.

### 6. Insert Program Label

Inserts label 1 into the iteration part of the program.

#### 7. Load Target Position

Loads the number of counts input by the operator, into the target position for the next move.

#### 8. Start Motion

Starts the motion of the axis.

#### 9. Add Variables

Adds the increment variable to the step counter variable and stores it in the step counter variable.

#### 10. Subtract Variables

Subtracts the step counter variable from the number of steps variable.

#### 11. Jump to Label on Condition

If the subtraction function performed in the previous step yields a number equal to or greater than 0, the program jumps to label 1.

#### 12. End Program Storage

Ends the storage of program 1 onboard Flexmotion.

#### 13. Run Program

Runs program 1 stored onboard Flexmotion.

#### 14. Status While Loop

While loop for monitoring the state of the onboard program.

## 15. Stop Program

Stops program 1 running onboard Flexmotion.

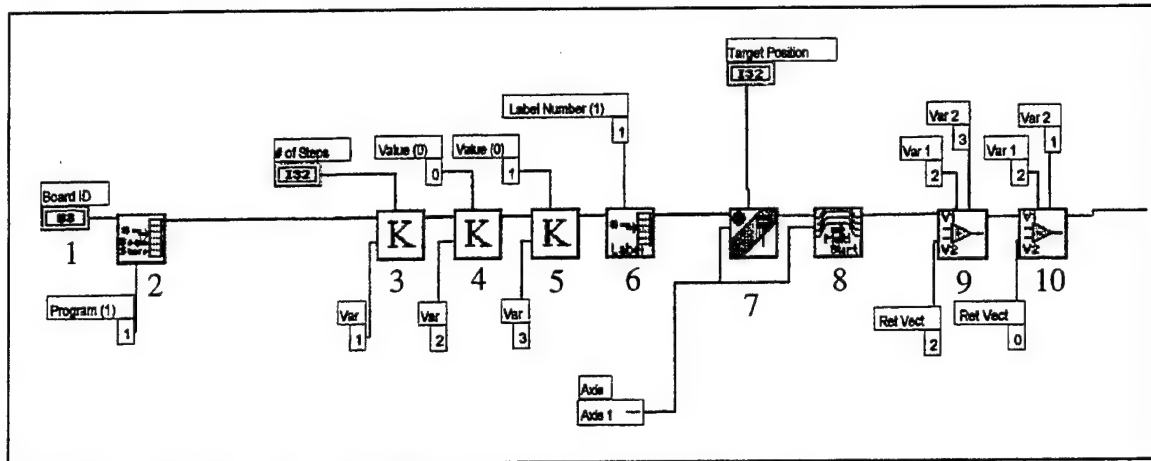


Figure B.3. Linus Stepping.vi.

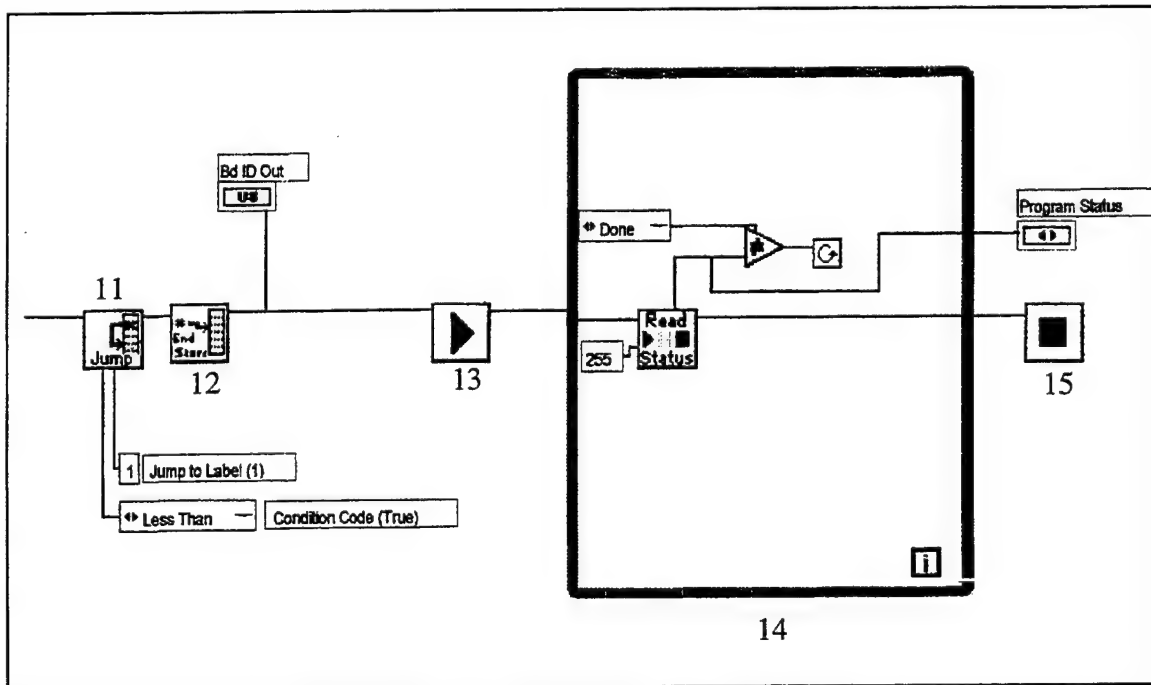


Figure B.4. Linus Stepping.vi (continued).

## APPENDIX C. SERVO TUNING PROCEDURE

This Appendix describes a general procedure to tune the servo system. A servo tuning LabView VI from the Flexmotion Library has been adapted for this purpose, and has been named "Linus Tuning.vi". The details of operation of the VI can be found in the online help. The program is stored in the same path mentioned in Appendix B.

The procedure here described is for time-domain step response tuning. Before executing the following procedure, trajectory parameters must be determined from the required profile of the motion, and input to the program.

Procedure:

1. Set the parameters  $K_I$ ,  $K_V$ ,  $A_{FF}$ , and  $V_{FF}$  to 0.
2. Set  $K_P$  to a low value ( $\approx 100$ ).
3. Set  $K_D$  to 10 times  $K_P$ .
4. Jog the motor and observe the response. Increase  $K_P$  and jog the motor until the rise time of the error does not improve.
5. Increase  $K_D$  until the maximum overshoot, and settling time are within required values.
6. If step 5 does not yield the required result, increase (in 1 unit increments)  $T_D$ . Each time  $T_D$  is adjusted steps 4 and 5 must be repeated.
7. Once rise time, overshoot, and settling time are in tolerance, increase  $K_I$  (in 1 unit increments) until the steady-state error is 0.

After much experimentation and analysis, the PID parameters listed in table C.1 were found to yield the best overall step response.

Control Parameter	Value
$K_P$	300
$K_I$	5
$I_L$	1000
$K_D$	4000
$T_D$	3
$K_V$	0
$A_{FF}$	0
$V_{FF}$	0

Table C.1. Control parameters.

## LIST OF REFERENCES

1. Marino, S.A., *Operation and Calibration of the NPS Ultraviolet Imaging Spectrometer (NUVIS) in the Detection of Sulfur Dioxide Plumes*, Master's Thesis, Naval Postgraduate School, Monterey, California, December 1999.
2. Hecht, E., *Optics*, Third Edition, Addison-Wesley Longman Inc., 1988.
3. Klein, M.V. and Furtak, T.E., *Optics*, Second Edition, John Wiley & Sons, 1986.
4. Pedrotti, F.L. and Pedrotti, L.S., *Introduction to Optics*, Second Edition, Prentice Hall, 1993.
5. Vanesse, G., *Spectrometric Techniques Volume I and II*, First Edition, Academic Press, 1977.
6. Hernandez, G., *Fabry-Perot Interferometers*, First Edition, Cambridge University Press, 1986.
7. Wolfe, W.L., *Introduction to Imaging Spectrometers*, First Edition, SPIE Optical Engineering Press, 1997.
8. ICS Advent, Chassis Manual, 00431-241-1C, *7490 Series*, 1999.
9. ICS Advent, Product Manual, 00431-020-4D, *ISA/PCI Backplanes*, 1999.
10. ICS Advent, Single Board Computer Manual, 00431-248-1C, *SB686BX Series*, 1999.
11. Princeton Instruments Inc., Operation Manual, 4411-0062, *Intensified Pentamax System*, 1997.



12. Princeton Instruments Inc., Operation Manual, 4411-0017, *PG-200 Programmable Pulse Generator*, 1997.
13. National Instruments, User Manual, 321944A-01, *Motion Control FlexMotion<sup>TM</sup> Hardware*, 1998.
14. National Instruments, User Guide, 321942A-01, *nuDrive Accesory*, 1998.
15. National Instruments, User Manual, 320999B-01, *LabVIEW<sup>TM</sup>*, 1998.
16. National Instruments, Reference Manual, 321296B-01, *G Programming*, 1998.
17. Kuo, B.C., *Automatic Control Systems*, Seventh Edition, Prentice Hall, 1995.
18. National Instruments KnowledgeBase, 1FMDEDKS, *Specification Issues When Using the Servo NuDrive with a Specific Motor*, 3 December 1998.

## INITIAL DISTRIBUTION LIST

1. Defense Technical Information Center ..... 2  
     8725 John J. Kingman Road, Suite 0944  
     Ft. Belvoir, VA 22060-6218
  
2. Dudley Knox Library ..... 2  
     Naval Postgraduate School  
     411 Dyer Road  
     Monterey, CA 93943-5101
  
3. David S. Davis Code PH/DV ..... 2  
     Department of Physics  
     Naval Postgraduate School  
     Monterey, CA 93943-5101
  
4. Richard C. Olsen Code PH/OS ..... 2  
     Department of Physics  
     Naval Postgraduate School  
     Monterey, CA 93943-5101
  
5. Chairman, Code PH..... 2  
     Department of Physics  
     Naval Postgraduate School  
     Monterey, CA 93943-5101
  
6. Curricular Officer Code 34..... 1  
     Engineering and Technology  
     Naval Postgraduate School  
     Monterey, CA 93943-5107
  
7. Ricardo Kompatzki ..... 4  
     1 Norte 1117  
     Vina del Mar  
     Chile, South America